



Multi-year, spatially extensive, watershed-scale synoptic stream chemistry and water quality conditions for six permafrost-underlain Arctic watersheds

Arial J. Shogren^{1,a}, Jay P. Zarnetske¹, Benjamin W. Abbott², Samuel Bratsman², Brian Brown², Michael P. Carey³, Randy Fulweber⁴, Heather E. Greaves⁴, Emma Haines¹, Frances Iannucci^{4,5}, Joshua C. Koch³, Alexander Medvedeff⁵, Jonathan A. O'Donnell⁶, Leika Patch², Brett A. Poulin^{7,8}, Tanner J. Williamson¹, and William B. Bowden⁵

⁸Arctic Network, National Park Service, Anchorage, Alaska 99501, USA

⁹Water Mission Area, U.S. Geological Survey, Boulder, Colorado 80303, USA

⁸Department of Environmental Toxicology, University of California Davis, Davis, California 95616, USA

^anow at: Department of Biological Sciences, The University of Alabama, Tuscaloosa, Alabama 35454, USA

Correspondence: Arial J. Shogren (shogrena@msu.edu)

Received: 2 May 2021 – Discussion started: 14 June 2021 Revised: 15 August 2021 – Accepted: 6 October 2021 – Published: 14 January 2022

Abstract. Repeated sampling of spatially distributed river chemistry can be used to assess the location, scale, and persistence of carbon and nutrient contributions to watershed exports. Here, we provide a comprehensive set of water chemistry measurements and ecohydrological metrics describing the biogeochemical conditions of permafrost-affected Arctic watersheds. These data were collected in watershed-wide synoptic campaigns in six stream networks across northern Alaska. Three watersheds are associated with the Arctic Long-Term Ecological Research site at Toolik Field Station (TFS), which were sampled seasonally each June and August from 2016 to 2018. Three watersheds were associated with the National Park Service (NPS) of Alaska and the U.S. Geological Survey (USGS) and were sampled annually from 2015 to 2019. Extensive water chemistry characterization included carbon species, dissolved nutrients, and major ions. The objective of the sampling designs and data acquisition was to characterize terrestrial-aquatic linkages and processing of material in stream networks. The data allow estimation of novel ecohydrological metrics that describe the dominant location, scale, and overall persistence of ecosystem processes in continuous permafrost. These metrics are (1) subcatchment leverage, (2) variance collapse, and (3) spatial persistence. Raw data are available at the National Park Service Integrated Resource Management Applications portal (O'Donnell et al., 2021, https://doi.org/10.5066/P9SBK2DZ) and within the Environmental Data Initiative (Abbott, 2021, https://doi.org/10.6073/pasta/258a44fb9055163dd4dd4371b9dce945).

1 Introduction

Watershed chemistry studies – like all ecosystem studies – involve trade-offs between sampling extent (i.e., how much area is observed) and spatiotemporal grain (i.e., the resolution of observations in space and time) (Abbott et al., 2018; Burns et al., 2019; Ward et al., 2019). Initial assessments are typically performed at the plot (terrestrial studies, < 1 to 100 m²) (Keller et al., 2007; Prager et al., 2017) or reach scales (stream studies, 100–1000 m), where replicated observations and manipulations can be made (Kling et al., 2000; Docherty et al., 2018). Trade-offs between extent and grain are especially apparent in remote settings such as the Arctic, where logistical constraints and high operational costs often force researchers to choose among these sampling approaches (Abbott et al., 2021). While these intensive studies are crucial to identifying the underlying processes controlling solute transport and transformations, it is challenging to scale up plot-level observations to the watershed, regional, or continental levels (Wiens, 1989; Thrush et al., 1997; Helton et al., 2012). Likewise, large-scale observations sensed remotely from aircraft or satellites often cannot identify the processes behind the regional to continental patterns they reveal (Newman et al., 2019; Shiklomanov et al., 2019). Bridging small- and large-scale observations is complicated by both spatial heterogeneity and temporal variation, as mosaics of diverse ecosystem patches evolve in space and time (Bernhardt et al., 2017; Pinay et al., 2015; Abbott et al., 2016). Consequently, mechanisms that are observed at the plot or regional levels may not reconcile (Kareiva and Andersen, 1988) because connectivity among patches can create emergent patterns and processes (Sivapalan, 2003; McDonnell et al., 2007; Covino, 2017). To understand and predict ecosystem behavior in the Anthropocene, we need to observe how biogeochemical patterns are produced and propagate across scales. Here, we describe a medium-scale watershed chemistry dataset that includes spatially distributed hydrological, ecological, and geochemical properties. Using a synoptic experimental design, we measured these parameters across medium-scale watersheds (< 1 to > 1000 km²) multiple times over several years. We hope this dataset will help bridge the gap between plot-level and regional investigation of ecosystem change in the permafrost zone.

Most water chemistry and flow assessments conducted in the Arctic and elsewhere are based on observations at river outlets (McClelland et al., 2006, 2007; Tank et al., 2016; Toohey et al., 2016; Shogren et al., 2020; Zarnetske et al., 2018). The flow of water integrates biogeochemical signals, such that river chemistry at the watershed outlet contains information about both terrestrial and aquatic biogeochemical processes that occurred upstream in the network (Temnerud et al., 2010; Vonk et al., 2019; Tank et al., 2020). Indeed, using sampling and monitoring approaches that capture the watershed outlet response over time has logistic and safety advantages for site access. Further, the recent applica-

tion of novel sensor technology has enabled high-frequency watershed-scale studies (Shogren et al., 2021; Ruhala and Zarnetske, 2017; Khamis et al., 2021). For example, the paired high-frequency flow and a limited set of chemical properties for the watersheds in this data paper are available at the Arctic Data Center (Zarnetske et al., 2020b, c, a). While these watershed outlet measurements can provide insight into possible upstream and upslope processes (Laudon et al., 2017; Shogren et al., 2021; Moatar et al., 2017), they often do not diagnose primary drivers of lateral transport of materials (Burns et al., 2019; Appling et al., 2018; Temnerud et al., 2010; Hoffman et al., 2013; Collier et al., 2018). These large-scale measurements are the result of variable inputs which are buffered and blurred as multiple spatiotemporal signals are mixed and propagated through the surface and subsurface network (Creed et al., 2015; Abbott et al., 2018; Kolbe et al., 2019). To identify the processes behind those signals, we need to venture into the headwaters, extending our observations into smaller subcatchments that match the spatial scale of mechanisms controlling carbon and nutrient uptake and release (Shogren et al., 2019; Gu et al., 2021; Abbott et al., 2017).

Spatially extensive or "synoptic" sampling frameworks, such as contained in this data paper, provide multi-scale information about the source of signals across the entire watershed network, creating a direct complement to watershed outlet monitoring. With a synoptic sampling design, researchers can capture the spatial extent of nested subcatchments and therefore assess terrestrial-aquatic transfer of material and stream network processing (Abbott et al., 2018; Shogren et al., 2019; Gu et al., 2021). Though synoptic campaigns are logistically challenging (Yi et al., 2010; Abbott et al., 2021; Rodríguez-Cardona et al., 2020), the highresolution spatial snapshot they generate allows empirical assessment of biogeochemical signals at intermediate spatial scales (Abbott et al., 2018; Shogren et al., 2019; McGuire et al., 2014). In recent years, synoptic campaigns have focused on solute distribution in temperate river systems (Gardner and McGlynn, 2009; McGuire et al., 2014; Byrne et al., 2017; Abbott et al., 2018; Dupas et al., 2019). While there have been fewer synoptic campaigns in permafrost systems (Kling et al., 2000; Bowden, 2013; Shogren et al., 2020; Abbott et al., 2015, 2021; Lamhonwah et al., 2017), their application presents an opportunity to characterize the fate of carbon and nutrients in a rapidly changing Arctic, creating multi-scale targets for the Earth system models used for predicting environmental change (Collier et al., 2018; Koven et al., 2015; Turetsky et al., 2020; Vonk et al., 2015). Because permafrost degradation is triggering both large-scale deepening of the active layer and discrete permafrost collapse (thermokarst) features (Gao et al., 2021; Turetsky et al., 2020; Farquharson et al., 2019), synoptic snapshots could be invaluable in detecting the degree, location, and type of climate response. Therefore, measuring the spatial distribution of water chemistry in high-latitude river networks could advance understanding of permafrost ecosystems and improve estimates of ecosystem feedbacks to climate change (Bring et al., 2016; Wrona et al., 2016; Schuur et al., 2015; Mu et al., 2020).

The datasets presented here were derived from repeated synoptic samplings in six Arctic watersheds in northern Alaska occurring on three distinct high-latitude ecosystem types: Arctic tundra, boreal forest, and Alpine tundra (Fig. 1). In this paper, we illustrate the utility of such data via a set of initial watershed chemistry analyses for ecologically significant reactive solutes including dissolved organic carbon (DOC), nitrogen (e.g., nitrate, N-NO₃⁻; ammonium, N-NH₄⁺; dissolved organic nitrogen, DON; total dissolved nitrogen, TDN), phosphorous (soluble reactive phosphorus, SRP; total dissolved phosphorus, TDP), and a suite of geochemically significant anions and cations (e.g., calcium, Ca²⁺; total iron, Fe; dissolved silica, DSi; see Table 1 for full list of analytes). In addition, we use these datasets to introduce simple metrics for biogeochemical solutes: variance collapse, subcatchment leverage, and spatial persistence (Abbott et al., 2018; Shogren et al., 2019; Gu et al., 2021; Dupas et al., 2019; Frei et al., 2020). These new metrics seek to extract information more fully from rich spatiotemporal water chemistry datasets. Specifically, these metrics characterize what spatial scale is the most relevant in explaining terrestrial-aquatic material flux, how much influence or leverage each sampling site has on the watershed budget, and whether individual samplings are adequate to capture temporal variation. In this light, synoptic sampling frameworks provide robust information about how to scale plot- and reach-level observations while also providing a multi-scale target for remotely sensed data and numerical models. Ultimately, the information gleaned from these metrics is desired by a range of disciplines from ecologists to natural resource managers.

First, we use subcatchment leverage to identify nested areas within the network that exert a disproportionate influence on flux at the watershed outflow (Abbott et al., 2018; Shogren et al., 2019). Subcatchment leverage can be interpreted as the contribution of the subcatchment to watershed mass flux where the value can be negative (indicating the subcatchment has lower areal flux than the outlet, decreasing watershed flux), positive (indicating the subcatchment has higher areal flux than the outlet, a net increase in flux), or zero (no influence because it is the same as the outlet). Estimating leverage allows identification of specific subcatchments with disproportionate influence on material export, defined here as high leverage. Subcatchments with high leverage behave as a strong source or sink within the watershed network, strongly influencing the resulting concentrations at the outflow, and can be selected as sites for further mechanistic study or monitoring. Likewise, the direction and magnitude of leverage averaged across the entire watershed contain information about net solute removal and production in the stream network (Shogren et al., 2019). For example, if the mean leverage

for the watershed is above zero, this indicates there are more solute sources than can be accounted for at the watershed outlet, implying there has been solute removal during transport through the network. Second, we examine what spatial extent or patch size controls solute production and removal by identifying thresholds of concentration variance collapse (Abbott et al., 2018). We generally expect the amplitude of solute variability to decrease moving downstream from headwaters to larger systems (Creed et al., 2015) with greater variability among headwaters, whereas downstream reaches are less likely to have extremely high or low concentrations because they integrate multiple upstream source or sink processes (Wolock et al., 1997; Temnerud and Bishop, 2005; Burt and Pinay, 2005; Abbott et al., 2017). Therefore, the size of nutrient sources and sinks in the landscape can be assessed by the spatial scale of the variance collapse of concentration among watershed reaches (Abbott et al., 2018; Shogren et al., 2019). The threshold of variance collapse is similar to the elementary representative area concept (Zimmer et al., 2013, p. 20), where the threshold represents the spatial scale at which landscape "patches" or processes throughout the watershed network that produce and remove solutes are effectively integrated. Lastly, the spatial persistence metric can be used to assess whether a given site is representative (i.e., the same pattern continues through time), or if patches restructure in space between sampling campaigns (i.e., reorganization of patches requires greater frequency in sampling) (Abbott et al., 2018; Dupas et al., 2019; Gu et al., 2021). Spatial persistence effectively quantifies the temporal representativeness of an instantaneous measurement at a given site, potentially indicating the type of process creating the patterns and informing future watershed study design and data analysis of extant data (Kling et al., 2000; Shogren et al., 2019).

2 Study location and design

2.1 Study watersheds

2.1.1 Arctic LTER sites at Toolik Field Station

The Arctic Long-Term Ecological Research (LTER) site based out of Toolik Field Station (TFS) is in the foothills of the Brooks Range on the North Slope of Alaska, USA (mean elevation 720 m). We conducted surveys in three watersheds near TFS: the Kuparuk River, Oksrukuyik Creek, and Trevor Creek. The three study watersheds were chosen because they spanned dominant circumarctic vegetation types, permafrost characteristics, and hydrologic conditions (Table 1). Further, the climate, morphology, and ecology of the sites and region have been previously described (Hobbie and Kling, 2014).

- The Kuparuk River (68.64816, -149.41152; Fig. 2a) is a meandering stream flowing through primarily tundra vegetation, located about 10 km northeast of TFS. The Kuparuk River includes a long-term monitoring site for the Arctic LTER, used as a site for ecological study and

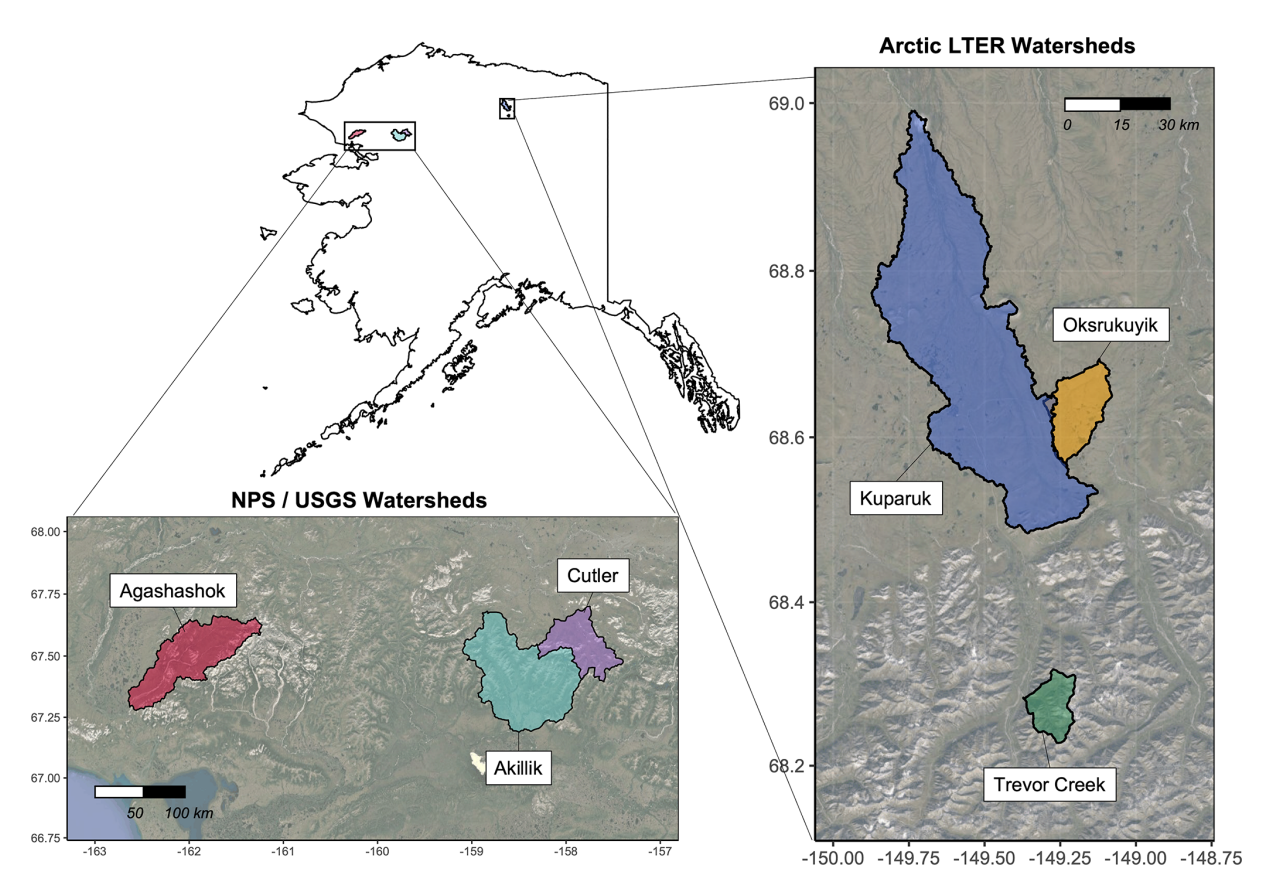


Figure 1. Regions of northern Alaska associated with the Arctic Long-Term Ecological Research site at Toolik Field Station (TFS) and National Park Service (NPS) and U.S. Geological Survey (USGS) watersheds. Map created in R Studio (version 1.2.1335) with base imagery from ESRI and © Google Earth (version 7.3.3.7786).

monitoring since 1979. From 1983–2016, the fourthorder reach of the Kuparuk River was used for a wholestream fertilization study (Peterson et al., 1993; Slavik et al., 2004; Iannucci et al., 2021), where phosphorous (H₃PO₄) was continuously added to assess response to nutrient fertilization. As the Kuparuk River continues north, it meets a large aufeis (ice) field (Yoshikawa et al., 2007; Terry et al., 2020).

- Oksrukuyik Creek (68.68740, -149.095, Fig. 2b) is a clear-water, low-gradient stream meandering through primarily tundra landscape, with intermittent presence of stream-lake connectivity (Shogren et al., 2019). Oksrukuyik Creek is also an Arctic LTER long-term monitoring site, approximately 20 km northeast of TFS.
- Trevor Creek (68.28482, -149.350063, Fig. 2c) is a mountainous alpine stream, draining into the Atigun River watershed, located 30 km south of TFS. Trevor Creek drains primarily steep, rocky slopes with limited heath and willow vegetation. The majority of stream runoff is generated by precipitation and snowmelt.

As a result of long-term study and a sustained commitment to data stewardship, the Arctic LTER and TFS hosts an ex-

tensive catalogue of terrestrial, aquatic, and atmospheric data that are complementary to the data presented in this publication. For more information, please see the LTER data catalogue (https://arc-lter.ecosystems.mbl.edu/data-catalog, last access: 15 August 2021), in addition to the abiotic and biotic monitoring data from the TFS Spatial and Environmental Data Center (https://toolik.alaska.edu/edc/index.php, last access: 15 August 2021).

2.1.2 National Park Service and U.S. Geological Survey sites

We also sampled three watersheds associated with the National Park Service (NPS) Arctic Inventory and Monitoring Network and a project funded by the U.S. Geological Survey's (USGS) Changing Arctic Ecosystem program. The Agashashok and Cutler River watersheds are within Noatak National Preserve, and the Akillik River watershed is within Kobuk Valley National Park. All three watersheds are situated near the northern extent of Alaska's boreal forest, where tree line is expanding (Suarez et al., 1999), and subcatchments vary in areal extent of forested versus tundra land cover. The study sites vary with respect to permafrost char-

Table 1. Summary of site characteristics for the watersheds where synoptic samplings were conducted. The descriptions are considered representative of the major landform types within the TFS and NPS/USGS watersheds.

	Site	Slope (°)	Mean elevation (m)	Geologic setting	Permafrost zone	Primary vegetation	Number of sampling sites	Total drainage area (km ²)
TFS	Kuparuk River	Low (3.1)	988	Sagavanirktok old Glaciated uplands	Continuous permafrost	Wet acidic tundra	45	92.5
	Oksrukuyik Creek	Low (3.2)	862	Sagavanirktok young Glaciated valleys	Continuous permafrost	Wet acidic tundra	42	72.6
	Trevor Creek	High (9.4)	1595	Sagavanirktok young Glaciated valleys	Continuous permafrost	Alpine valley	35	42.7
NPS/USGS	Agashashok River	High (9.3)	317	Sedimentary carbonate and non-carbonate lithology	Continuous permafrost	Boreal spruce forest, arctic tundra	9	1058.0
	Cutler River	High (8.0)	644	Quaternary, non-carbonate deposits (glaciolacustrine)	Continuous permafrost	Boreal spruce forest, arctic tundra	6	566.7
	Akillik River	High (14.8)	447	Quaternary, silt and peat	Discontinuous permafrost	Boreal spruce forest, arctic tundra	5	262.1

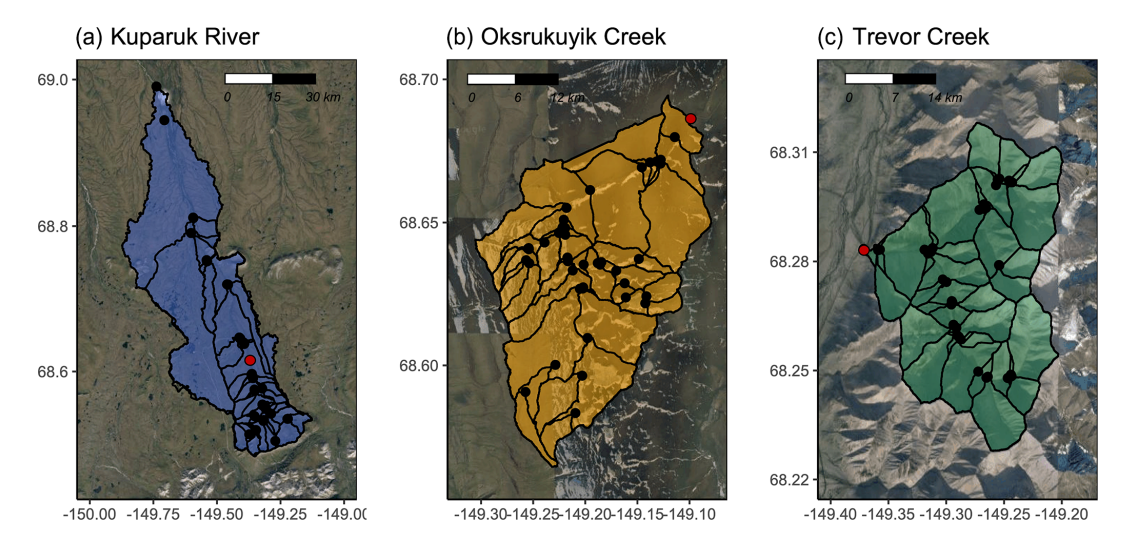


Figure 2. Synoptic sampling sites (black points) with subcatchment delineations from three watersheds related to the Arctic Long-Term Ecological Research site at Toolik Field Station (TFS) on the North Slope of Alaska. Study watersheds include the **(a)** Kuparuk River (blue), **(b)** Oksrukuyik Creek (orange), and **(c)** Trevor Creek (green). Scale bars in kilometers. The Arctic LTER monitoring stations are denoted by red points and described further in Shogren et al. (2021). Map created in R Studio (version 1.2.1335) with base imagery from ESRI and © Google Earth (version 7.3.3.7786).

acteristics, including soil texture, ground ice content, and subsurface hydrology (O'Donnell et al., 2016). Evidence suggests stream chemistry varies across these watersheds, including the form, amount, and age of dissolved carbon (O'Donnell et al., 2020).

- The *Cutler River* (67.845, −158.316, Fig. 3a) flows north out of the Baird Mountains through gently rolling

tundra into the upper Noatak River. The watershed is underlain by ice-rich glaciolacustrine deposits (O'Donnell et al., 2016), and soils tend to be organic-rich and poorly drained. Vegetation is dominated by moist acidic tundra and wet sedge meadows.

- The Akillik River (67.201, -158.572, Fig. 3b) flows south out of the Baird Mountains and into the Kobuk River downstream of the village of Ambler, Alaska. The river passes through alpine terrain in the headwaters before draining terrain comprised of ice-rich loess in the lower reaches. Vegetation is a mixture of boreal spruce forests and tundra.
- The Agashashok River (67.268, -162.636, Fig. 3c) is a braided, clearwater river that flows from the northeast to southwest into the lower Noatak River north of Kotzebue, Alaska. The headwaters drain rocky, alpine tundra terrain of the western Brooks Range. Downstream, the river drains broader valleys with a mixture of boreal spruce forest and tundra vegetation. The watershed is underlain by shallow bedrock, and permafrost is generally ice-poor (O'Donnell et al., 2016).

2.2 Synoptic sampling campaign design

2.2.1 Arctic LTER sites

Our sampling of the TFS watershed networks was designed to capture 30–50 nested subcatchments within the Kuparuk River, as well as Oksrukuyik and Trevor creeks. Site selection was based primarily on (1) presence of flowing surface waters, (2) representation across varying subcatchment drainage areas, and (3) site accessibility. Often, we a priori chose sites located at subcatchment confluences, sampling both upstream locations and then downstream of river mixing. In each of the TFS watersheds, we performed five repeated synoptic campaigns, sampling each stream network in August 2016, June 2017, August 2017, June 2018, and August 2018 (exact dates in Table 2). We accessed sampling sites either on foot or by helicopter within a 6 h period.

2.2.2 NPS/USGS sites

Sampling of the NPS/USGS watershed networks was designed to capture ~ 5 –10 subcatchments within the Agashashok, Cutler, and Akillik rivers. Sites were selected to span a gradient of size (subcatchment area, stream order), vegetation (forest vs. tundra), and permafrost characteristics (parent material, ground ice content). Due to variation in watershed aspect, streams also spanned a spatial gradient in permafrost ground temperatures, areal extent, and active layer thickness (Panda et al., 2016; Sjöberg et al., 2021). In addition to stream chemistry parameters, stream discharge was measured, and samples were collected to characterize stream biota (benthic biofilm, macroinvertebrates, and resident juvenile fish).

In each of the NPS/USGS watersheds, we performed 4–10 repeated synoptic campaigns, sampling each stream network in June, August, and September 2015; June, August, and September 2016; June and August 2017; and June and

August or September 2018 (exact dates in Table 2). We accessed sampling sites by helicopter within a 24 to 96 h period

3 Methods

3.1 Synoptic site characterization

3.1.1 Subcatchment delineation for drainage area

The location of each stream sampling site was recorded in a spreadsheet and imported into GIS software (ESRI ArcGIS v. 10.4). These sites served as starting points ("pour points") from which watersheds and subcatchments were delineated following the general procedure described here: https://support.esri.com/en/technical-article/000012346 (last access: 1 May 2018). The following two digital elevation models (DEMs) were needed to cover the spatial distribution of the stream sampling sites and were used to create the necessary flow direction and flow accumulation layers: Arctic-DEM from the Polar Geospatial Center (Porter et al., 2018) and ASTER GDEM v.2 (NASA/METI/AIST/Japan Space Systems and US/Japan ASTER Science Team, 2009). A Python script was written to iterate over the list of sample sites and execute the watershed delineation procedure.

3.1.2 Estimation of terrestrial catchment characteristics for TFS sites

We characterized the terrestrial environment of the TFS sites using remotely sensed data pertaining to the vegetation and topography of each subcatchment. For each subcatchment polygon, we extracted the mean, standard deviation, and range of the elevation, slope, and topographic position index (i.e., the elevation of a given pixel relative to surrounding pixels, sometimes known as slope position). These metrics were calculated from 25 m resolution elevation data retrieved from the USGS National Map website (https://viewer. nationalmap.gov/basic/, last access: 1 May 2018). The normalized difference vegetation index (NDVI), which indicates the presence of green vegetation, was derived from imagery acquired in summer 2012 by the ETM+ sensor on Landsat 7 (courtesy of the USGS). We also extracted percent cover of vegetation classes in each subcatchment from the 30 m resolution Jorgenson northern Alaska ecosystems map (Muller et al., 2018). All data extraction was performed using zonal statistics via ArcPy (ESRI, 2016) in Python.

3.2 Water sampling and analysis

3.2.1 Field sample collection and preparation

Arctic LTER

During each synoptic campaign, at each site we measured in situ physiochemical variables (this section) and sampled stream surface water for chemical analysis (Sect. 3.2.2). All

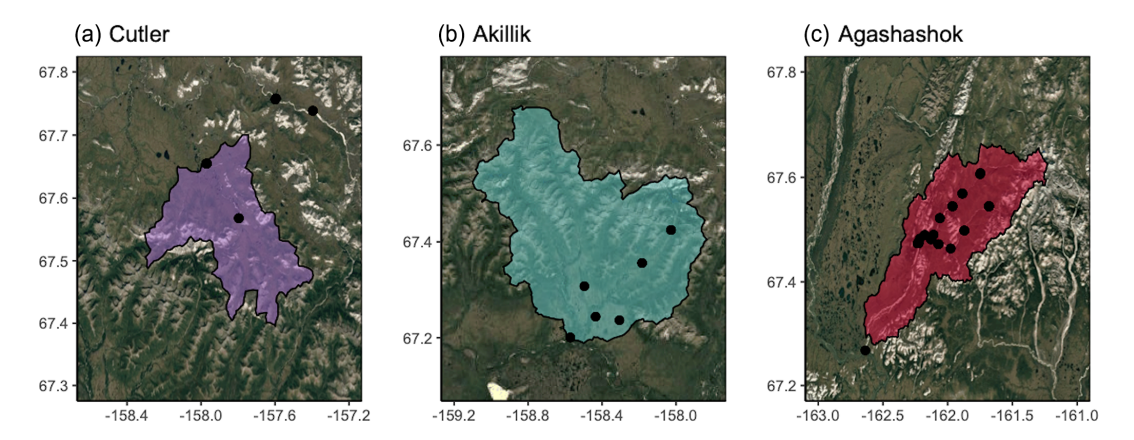


Figure 3. Synoptic sampling sites in three NPS/USGS watersheds. Study watersheds include the (a) Cutler, (b) Akillik, and (c) Agashashok rivers. Map created in R Studio (version 1.2.1335) with base imagery from ESRI and © Google Earth (version 7.3.3.7786).

Table 2. Description of the sampling campaign regimes, including dates for each campaign, for the TFS and NPS/USGS watersheds.

	Site	Years of repeated synoptic sampling	Number of sampling events	Sampling dates	Seasonal sampling
TFS	Kuparuk River	2016–2018	5	2016: 8/26 2017: 6/5; 8/27 2018: 6/6; 8/24	June, August
	Oksrukuyik Creek	2016–2018	5	2016: 8/17 2017: 6/3; 8/24 2018: 6/4; 8/23	June, August
	Trevor Creek	2016–2018	5	2016: 8/22 2017: 6/7; 8/31 2018: 6/8; 8/28	June, August
NPS/USGS	Agashashok River	2015–2019	10	2015: 6/9–6/12; 8/7–8/11; 9/16–9/19 2016: 6/7–6/12; 8/9–8/12; 9/8–9/9 2017: 6/6–6/8; 8/16–8/18 2018: 6/11–6/12; 9/2–9/6	June, August, September
	Cutler River	2015–2019	5	2016: 8/14–8/15 2017: 6/10; 8/20–8/21 2018: 6/14; 8/31–9/1	June, August, September
	Akillik River	2015–2019	4	2017: 6/11–6/12; 8/22–8/23 2018: 6/13; 8/302017: 6/11–6/12; 8/22–8/23	June, August, September

physical water samples were grab sampled directly from the stream thalweg, or as close to mid-channel as could be safely accessed. We collected samples in acid-washed and triplerinsed 1 L amber high-density polyethylene (HDPE) bottles. We used handheld YSI ProPlus multiparameter probes (YSI Instruments part no. 626281) and YSI ProODO dissolved oxygen meter (YSI Instruments part no. 6050020) to measure specific conductance (μ S cm⁻¹), pH, temperature (°C), and dissolved oxygen (DO, in percent saturation and mg O₂ L⁻¹) at each sampling site. We placed the probe into the water column where the water sample was taken and waited for the

temperature and DO readings to stabilize before recording the final value.

Upon returning to the lab at TFS, we processed each water sample into aliquots for specific analytes within 8 h of collection. We lab-filtered samples for dissolved water chemistry and nutrients using handheld 60 mL syringes. We triple-rinsed syringes with unfiltered sample water. Then, we sparged each filter cartridge with $\sim 10\,\mathrm{mL}$ of sample water prior to sample filtration; we used the sparge volume as the initial bottle rinse. We filtered samples for DOC and TDN into triple-rinsed amber 60 mL HDPE bottles using a

25 mm 0.2 μ m cellulose acetate filter (Sartorius CA membrane, 11107-25-N). We filtered samples for dissolved nutrients, anions, and cations into triple-rinsed clear HDPE 60 mL bottles using a 47 mm 0.7 μ m glass fiber filter (Whatman GF/F, 1825-047). Additionally, we placed ~ 60 mL of unfiltered sample water into a clear HDPE bottle for analysis of turbidity (NTU) and alkalinity (mg CaCO₃ L⁻¹). After processing, we froze samples at -4 °C until analysis, except for aliquots for DOC and total dissolved nitrogen (TDN). We stored DOC and TDN samples at 2 °C until analysis. Samples were shipped express to the University of Vermont (UVM) and Brigham Young University (BYU) for further analysis.

NPS/USGS

While sample collection and processing were similar between the TFS and NPS/USGS field sites, the filtration step varied slightly. For NPS/USGS samples, we followed standard USGS protocols. We filtered all samples for nutrient, anion, and cation analysis using 0.45 µm capsule filters (Geotech Versapor dispos-a-filter) into 250 or 500 mL HDPE bottles. We filtered samples for DOC and TDN into 125 mL amber glass bottles. Samples for alkalinity and total Fe were left unfiltered. DIC samples were collected without filtering or any headspace in 60 cc Luer-lock syringes fit with twoway stopcocks. After processing, we froze samples at -4 °C until analysis, with the exception of aliquots for DOC, TDN, and DIC that were stored at 2 °C until analysis. Samples were shipped express to Oregon State University's Cooperative Chemical Analytical Laboratory (CCAL) or the USGS in Boulder, Colorado, for further analysis.

3.2.2 Dissolved water chemistry analysis

Arctic LTER

We include further detail on analytical methods and instrumentation in Table 3, though we briefly describe our methods here. We measured DOC (as non-purgeable organic carbon, nPOC) and total dissolved nitrogen (TDN) with a total carbon analyzer (Shimadzu TOC-LCPH with a total nitrogen analyzer and ASI-L autosampler). We determined dissolved organic matter (DOM) optical properties including the spectral ratio $(S_r, unitless)$ and specific ultraviolet absorbance at 254 nm (SUVA₂₅₄) from the TOC and TN dataset (Helms et al., 2008; Hansen et al., 2016). We colorimetrically analyzed SRP, particulate phosphorous (PP), and total dissolved phosphorous (TDP) on a spectrophotometer (Shimadzu UV-2600). We quantified inorganic nitrogen species (nitrate, NO₃; ammonium, NH₄⁺) using a flow-through injection analysis (Lachat QuikChem flow injection analysis system). We measured several cations (Na $^+$, Li $^+$, K $^+$, Mg $^{2+}$, Ca $^{2+}$, NH $_4^+$), anions (F $^-$, Cl $^-$), oxoanions (NO $_2^-$, SO $_4^{2-}$, NO $_3^-$, PO₄³⁻), and organic acids (acetate, CH₃COO⁻; and formate, HCOO⁻) on an ion chromatography system (Thermo Fisher Scientific Dionex ICS5000). We quantified other geogenic anions and cations (e.g., Al^{3+} , As^{3-} , B^{3-} , Ba^{2+} , Br^+ , Ca^{2+} , Cd^{2+} , Co^{2+} , CrO_4^- , nominally dissolved Cu and Fe, K^+ , MoO_3^{2-} , Mg^{2+} , Mn^{2+} , Na^+ , Ni^{2+} , P, Pb^{2+} , P, Pb^{2-} , P, Pb^{2-} , Pb^{2-} ,

NPS/USGS

We include further detail on analytical methods and instrumentation in Table 3. For the NPS/USGS sites, we measured DOC and DIC (OI Analytical Model 700 TOC analyzer and Shimadzu TOC-VCSH combustion analyzer, respectively). We characterized DOM aromaticity by measuring UV-visible absorbance on filtered stream water samples on an Agilent model 8453 photodiode array and then calculating SUVA₂₅₄ (Weishaar et al., 2003). We also measured TDN and TDP on a Technicon AutoAnalyzer II. We quantified inorganic nitrogen species (NO₃⁻ + NO₂⁻ and unionized NH₃) and orthophosphate (PO₄³⁻) using a flow-through injection analysis system (Lachat QuikChem 8500). We calculated alkalinity using a titration to a pH of 4.5, using 0.02 N Na₂CO₃ and 0.02 N H₂SO₄ (ManTech PC-Titrate auto titrator system). Finally, we used ion chromatography to measure Cl⁻ and SO₄²⁻ (Dionex 1500 IC) and absorption spectroscopy to measure Na+, K+, Mg2+, Ca2+, and total Fe (Shimadzu AA-7000).

3.3 Estimation of ecohydrological metrics

In addition to reporting solute concentrations for each synoptic campaign (e.g., Figs. 4 and 5), we estimated ecohydrological metrics for each nested site and watershed. Across these analyses, we assigned any value below detection as the values of half the limit of quantification and kept these data points in the analysis. When the sample was not run for a specific solute, the cell was left blank.

3.3.1 Subcatchment leverage

First, we estimated *subcatchment leverage* from each of the synoptic sampling events for each solute. Subcatchment leverage is calculated as the difference in terms of concentration at each site (C_s) from the concentration at the watershed outlet (C_o) , subcatchment area (A_s) relative to the entire watershed area (A_o) , and specific discharge at the sampling location $(q = Q_s/A_s)$, where Q_s and A_s are the discharge and subcatchment area at the sampling point):

specific subcatchment leverage =
$$\left[(C_s - C_o) \cdot \frac{A_s}{A_o} \cdot q \right]$$
. (1)

Table 3. Summary of sample processing and analytical methods used for the dataset for (a) TFS and (b) NPS/USGS field sites.

(a) TFS					
	Parameter	Units	Instrument	Analytical method	Detection limit
Watershed characteristics	Drainage area	km ²			
	Slope (mean)	Degrees			
	Slope (standard deviation)	Degrees	Arc-GIS	Spatial analysis	
	Roughness (mean)	NDVI			
	Roughness (standard deviation)	NDVI			
Water quality measurements	Temperature	J _o	YSI Pro Plus multiparameter meter	Analyzed in the field with a handheld field probe	
	Specific conductivity	$\mu S cm^{-1}$			
	Hd	Hd			
	0 ₂	% Sat	YSI ProODO dissolved oxygen meter		
Water chemistry (post-filtering)	Turbidity	NTU	Forest Technology Systems (FTS) DTS-12 digital turbidity sensor	Nephelometric geometry	0.2 NTU
	DOC	Μμ	Shimadzu TOC-LCPH with TN	Combustion catalytic oxidation method	0.3 µM
	TDN	Μμ		High-temperature catalytic combustion and chemiluminescence detection	0.28 µМ
	N-NO ₃	Μμ	Lachat QuikChem flow	Cadmium reduction	0.03 µM
	N-NH ₄	Μμ	injection analysis system	Sodium salicylate-based procedure that requires a standard heating unit and is read at 660 nm	0.3 µМ
	SRP	Μμ	Shimadzu UV-2600 spectrophotometer	Colorimetric analysis using an ammonium molybdate-based reagent (although technically USGS refers to this as the ascorbic acid method)	0.05 µМ
	PP	Μπ		Same as above, preceded by combustion at 500°C and a hydrochloric acid digestion	0.05 µM
	TDP	Μμ		Same as SRP, preceded by a potassium persulfate digestion	0.05 µM
	F. acetate, formate, Cl, NO ₂ , Br, SO ₄ , PO ₄ , Li, Na, NH ₄ , K, Mg, Ca	Ми	Thermo Scientific Dionex ICS-2100 integrated IC system with electrolytic eluent generation with an AS-AP autosampler	Ion chromatography	0.05 µМ
	пРОС	${ m mgL}^{-1}$	Shimadzu TOC-LCPH with TN	Combustion catalytic oxidation method	0.3 µM
	Spectral slope ratio	Unitless			
	SUVA ₂₅₄	$\rm LmgC^{-1}m^{-1}$			
	Al, As, B, Ba, C, Cd, Co, Cr, Cu, Fe, K, Mg, Mn, Mo, Na, Ni, P, Pb, S, Se, Si, Sr, Ti, V, Zn	Ми	ICP-MS	Inductively coupled plasma mass spectrometry (ICP)	$0.02\mathrm{mgL^{-1}}$
	Alkalinity	meqL^{-1}	Accumet AB200 pH meter	Samples individually titrated with 0.18 N sulfuric acid	$0.2~\mathrm{meq}\mathrm{L}^{-1}$

Table 3. Continued.

(2)					
Par	Parameter	Units	Instrument	Specific method	Detection limit
Watershed Dra	Drainage area	km ²	Arc-GIS	Watershed delineation	
characteristics Slo	Slope (mean)	Degrees			
Slo	Slope (standard deviation)	Degrees			
Roi	Roughness (mean)	NDVI			
Roi	Roughness (standard deviation)	NDVI			
Water quality Ter	Temperature	°C	YSI Pro Plus multiparameter meter		
measurements Spe	Specific conductivity	$\mu \mathrm{S}\mathrm{cm}^{-1}$			
(taken in the field) pH		pН			
O_2		% Sat	YSI ProODO dissolved oxygen meter		
Water chemistry DOC (post-filtering)	C	mgL^{-1}	OI Analytical Model 700 TOC analyzer	Platinum-catalyzed persulfate wet oxidation method	4 μg
TDN	Z	mgL^{-1}	Technicon AutoAnalyzer II	Persulfate digest	$0.01{\rm mgL^{-1}}$
NC	$NO_3 + NO_2$	mgL^{-1}	Lachat QuikChem 8500	Cadmium reduction	$0.001{ m mg}{ m L}^{-1}$
NH ₄	4	mgL^{-1}		Colorimetric	$0.01{\rm mgL^{-1}}$
SRP	Ρ	mgL^{-1}		Ascorbic acid method	$0.001\mathrm{mg}\mathrm{L}^{-1}$
TDP	P	mgL^{-1}	Technicon AutoAnalyzer II	Persulfate digest	$0.002\mathrm{mg}\mathrm{L}^{-1}$
CI,	Cl, SO ₄	mgL^{-1}	Dionex 1500 IC	Ion chromatography	$0.01{ m mg}{ m L}^{-1}$
Na	Na, K, Mg, Ca, Fe	$ m mgL^{-1}$	Shimadzu AA-7000	Flame atomic absorption spectroscopy	$0.01, 0.03, 0.02, \\ 0.06, 0.06 \mathrm{mg} \mathrm{L}^{-1}$
SU	SUVA ₂₅₄	$LmgC^{-1}m^{-1}$		Spectrophotometer	
AH	Alkalinity	mgCaCO ₃ L ⁻¹	ManTech PC-Titrate auto titrator system	Titration to 4.5, use 0.02 N Na ₂ CO ₃ and 0.02 N H ₂ SO ₄	$0.2\mathrm{mg}\mathrm{CaCO_3}\mathrm{L}^{-1}$
DIC		mgL^{-1}	Shimadzu TOC-VCSH combustion analyzer	Combustion catalytic oxidation method	$0.05\mathrm{mg}\mathrm{L}^{-1}$

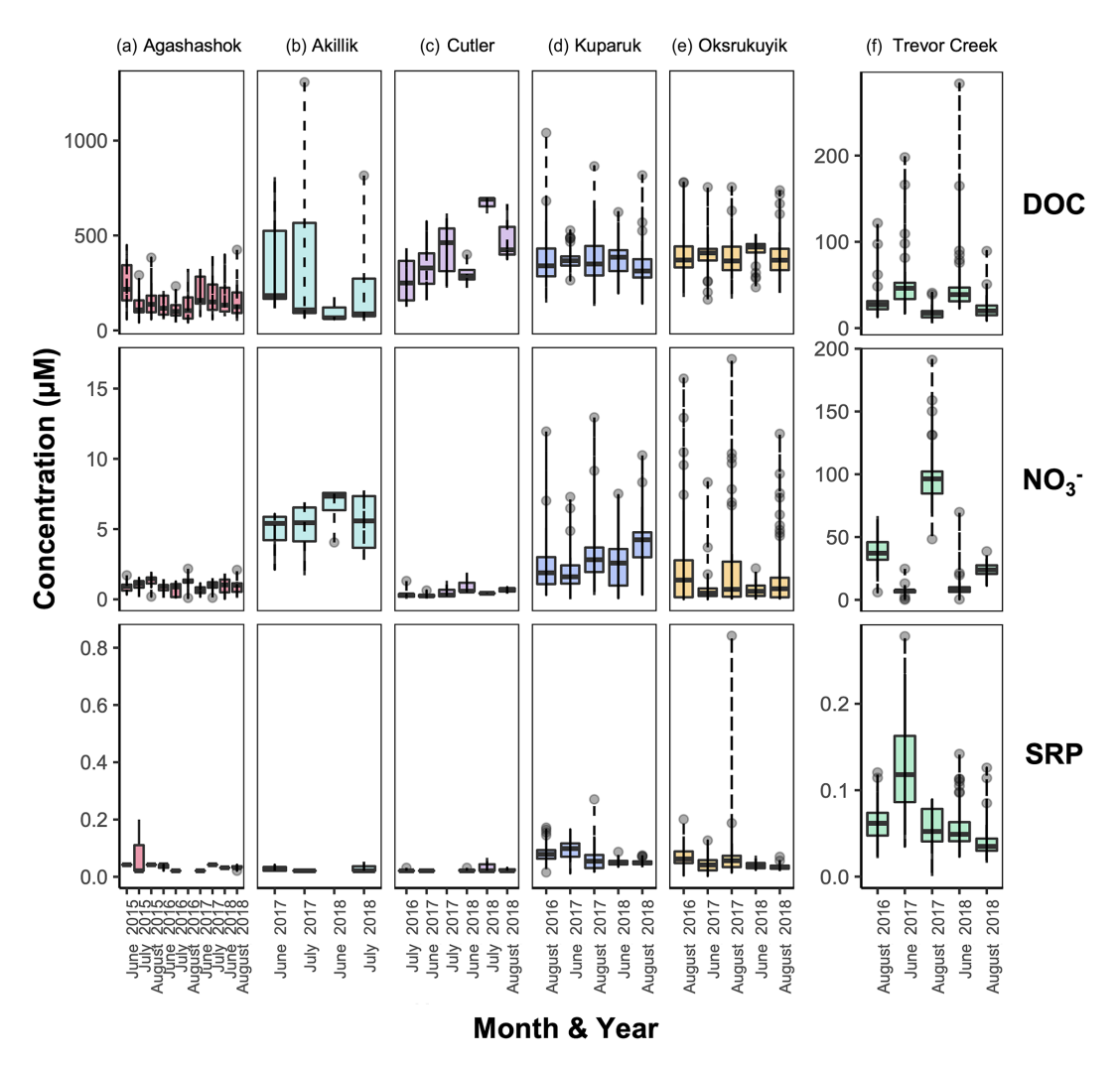


Figure 4. Boxplots of dissolved organic carbon (DOC, top row), nitrate (NO_3^- , middle row), and soluble reactive phosphorus (SRP, bottom row) concentration ranges (in μ M) in the (a) Agashashok River, (b) Akillik River, (c) Cutler River, (d) Kuparuk, (e) Oksrukuyik Creek, and (f) Trevor Creek watersheds across all years and seasons sampled. Each box encapsulates values within the lower 25th and upper 75th quartiles respectively, while the whiskers represent the minimum and maximum quartiles. Within each box, the horizontal line represents the median leverage value. Data points outside the whiskers represent values above and below $1.5\times$ the interquartile range (IQR) threshold.

In the case of Eq. (1), leverage is expressed in units of flux (mass/volume/time). However, if specific discharge is unavailable for each sampling location, leverage can be estimated using only variability in concentration and subcatchment area, so long as specific discharge (q) is similar between subcatchments (Asano et al., 2009; Karlsen et al., 2016). With the exception of the Agashashok River, which has flow generated from deeper flow paths, our study watersheds have very little regional groundwater influence (Lecher, 2017), and the synoptic campaigns were performed near base-flow conditions. Therefore, for the purposes of this study, we assumed that q was similar for subcatchments within a study watershed but not necessarily across the six study watersheds. This assumption was tested at all Arctic LTER sites using dilution gauging at a subset of sites in sum-

mer 2018 and 2019, where we found that values of specific discharge were similar across subcatchment sizes (Arial J. Shogren, unpublished data). We used Eq. (2) to estimate subcatchment leverage for all sampling locations across sampling events:

subcatchment leverage (%) =
$$100 \cdot \left[(C_s - C_o) \cdot \frac{A_s}{A_o} \right]$$
. (2)

Here, subcatchment leverage has units of concentration, or percentage when normalized to outlet concentration. In other words, the distributed mass balance is relative to a predetermined outflow point; with the presented analysis, we used the furthest downstream point with the largest drainage area as our outlet location. The interpretation of leverage values is opposite at the site and watershed scales (Abbott et al., 2018; Shogren et al., 2019). For example, a site

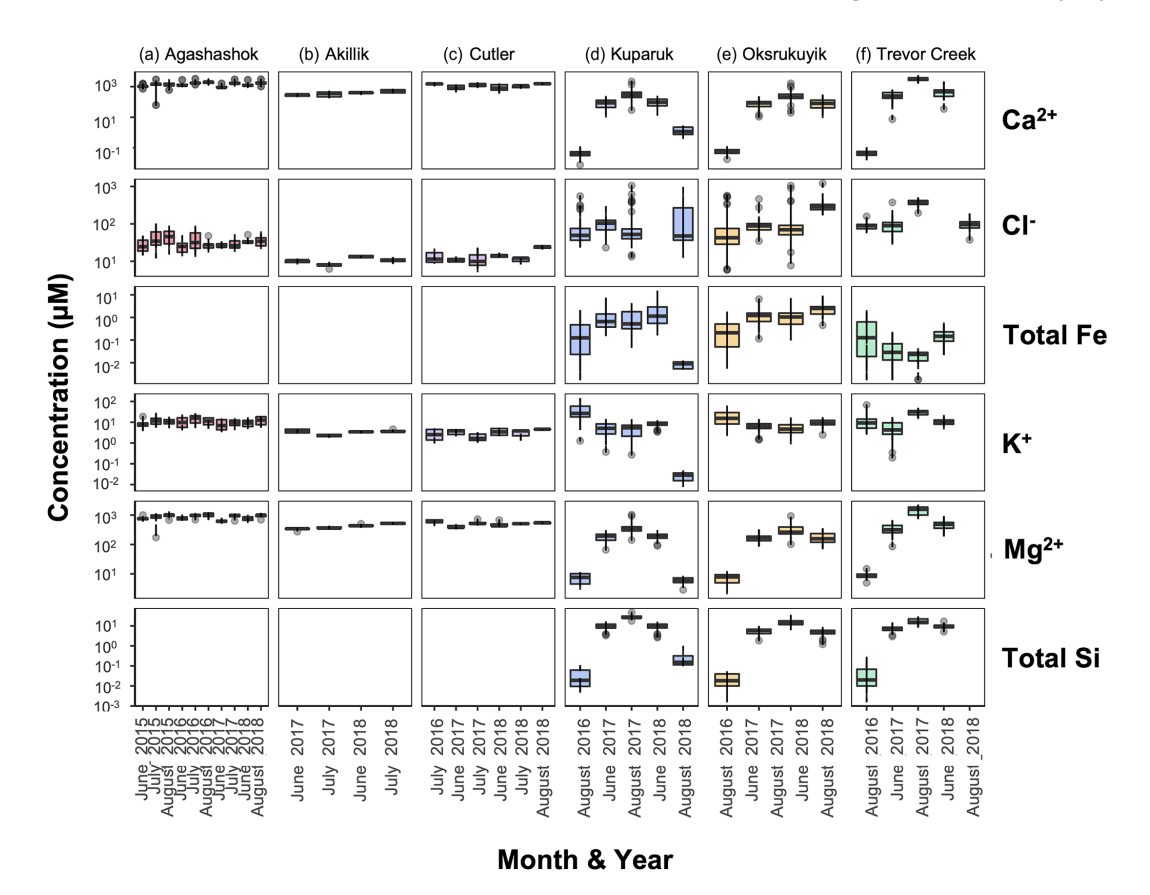


Figure 5. Boxplots of Ca^{2+} , Cl^- , Fe (total for NPS/USGS; nominally dissolved for TFS), K^+ , Mg^{2+} , and total Si concentration ranges (in μ M) in the (a) Agashashok River, (b) Akillik River, (c) Cutler River, (d) Kuparuk River, (e) Oksrukuyik Creek, and (f) Trevor Creek watersheds across all years and seasons sampled. Each box encapsulates values within the lower 25th and upper 75th quartiles respectively, while the whiskers represent the minimum and maximum quartiles. Within each box, the horizontal line represents the median leverage value. Data points outside the whiskers represent values above and below $1.5\times$ the IQR threshold.

with a positive value for subcatchment leverage is contributing more than the typical subcatchment in the watershed. Conversely, a watershed with a mean leverage value that is positive is indicative of a net removal in the stream network because there is more solute in the tributaries than can be accounted for at the watershed outlet, while a negative value suggests solute production in the network (Abbott et al., 2018; Shogren et al., 2019). We report both mean leverages for each catchment (presented in Figs. 6 and 7) and site-specific subcatchment leverages for each solute (Fig. 10 for DOC and NO₃⁻, but all other solutes can be found within the ecohydrological metrics datasets).

3.3.2 Concentration variance collapse

Next, to assess the representative patch size where concentration variance is reduced, we determined the threshold of concentration *variance collapse* for each solute from each synoptic sampling event (shown in Fig. 8). Using concentrations plotted over watershed area, we used the changepoint package in R (Killick and Eckley, 2014) to determine the collapse in variance of concentration across the whole water-

shed area. To determine the reduction in variance statistically, we used the pruned exact linear time (PELT) method, which compares differences in data points to determine statistical breakpoints (Abbott et al., 2018; Shogren et al., 2019). We performed this analysis using scaled concentrations, which were scaled by subtracting the whole watershed mean and dividing by the standard deviation to facilitate comparison of changes in variance and evaluate convergence towards the watershed mean. The variance collapse threshold is therefore expressed in units of area (here as km²). A non-significant variance collapse threshold can be interpreted to mean either the processes controlling lateral fluxes are operating at too small or too large a scale to be captured using a subcatchment sampling approach.

3.3.3 Spatial persistence

Lastly, we analyzed this spatially rich synoptic data to quantify the *spatial persistence* of stream nutrient concentrations and to determine the level of sub-grid resolution necessary to represent controls on lateral nutrient loss. The spatial persistence metric indicates whether spatial sampling is represen-

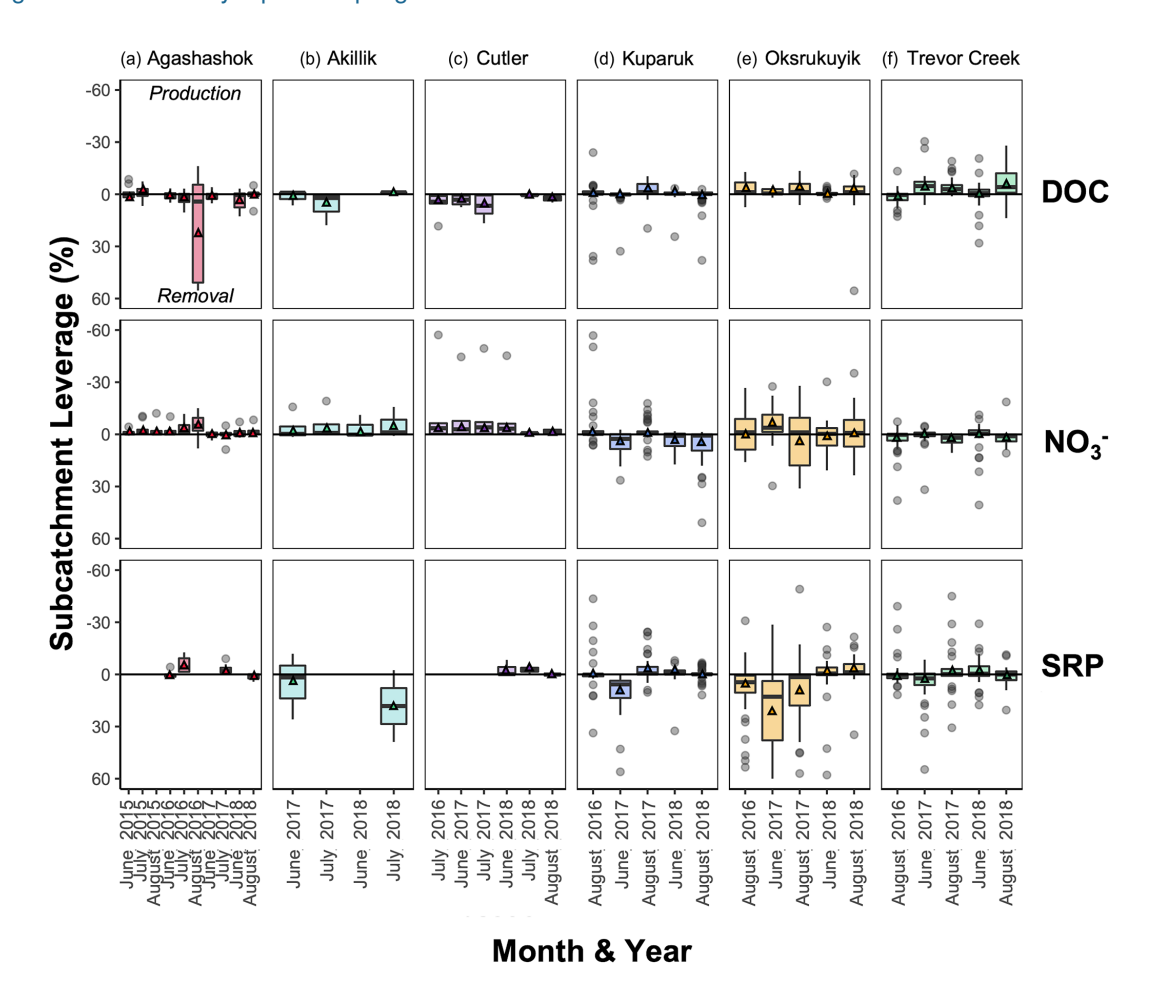


Figure 6. Boxplot of subcatchment leverage for select reactive solutes (DOC, NO_3^- , and SRP) in the (a) Agashashok River, (b) Akillik River, (c) Cutler River, (d) Kuparuk River, (e) Oksrukuyik Creek, and (f) Trevor Creek watersheds across all years and seasons sampled. Note reversed axes for ease of interpretation: negative values above the 0 line indicate production; positive values below the 0 line indicate removal. Each box encapsulates values within the lower 25th and upper 75th quartiles respectively, while the whiskers represent the minimum and maximum quartiles. Within each box, the horizontal line represents the median leverage value and the colored triangle lies at the mean. Data points outside the whiskers represent values above and below $1.5 \times$ the IQR threshold.

tative or whether spatial patterns reshuffle over time. Spatial persistence (r_s) is calculated as

$$(r_s) = \left(\frac{\text{covariance}(\text{rg}_x, \text{rg}_y)}{\sigma_{\text{rg}_x}\sigma_{\text{rg}_y}}\right),\tag{3}$$

where rg_x is the rank of subcatchments at the time of synoptic sampling, rg_y is the rank of the long-term flow-weighted concentrations, while σ_{rg_x} and σ_{rg_y} are the standard deviation of the rank variables. We calculated spatial persistence using the correlation function in R (version 3.3.0), using the Spearman method (Abbott et al., 2018; Shogren et al., 2019). Significance was tested using a Student t distribution test. Additional methods for calculating spatial persistence have now been proposed that do not require discharge data for the flow weighting (Gu et al., 2021). For the purposes of the Arctic LTER analysis, we estimated spatial persistence as the Spearman's correlation between early (June) and late (August) site

concentrations, resulting in a single spatial persistence metric (r_s) for 2017 and 2018. For the NPS/USGS sites, spatial persistence was calculated as the correlation between site locations sampled in the early (June) and mid (July) and the mid to late (August or September) seasons.

3.4 Use and interpretation of ecohydrological ecosystem metrics

The original intent of this paper was to present our unique Arctic datasets and showcase the utility of a synoptic framework in combination with metrics that describe the spatial distribution of river chemistry. To further highlight how these metrics can inform future sampling design and address fundamental ecological questions, below we describe patterns for DOC and NO₃⁻ in the TFS watersheds.

For solutes, the spatial variability in concentration depends on the strength and connectivity of both source and sink

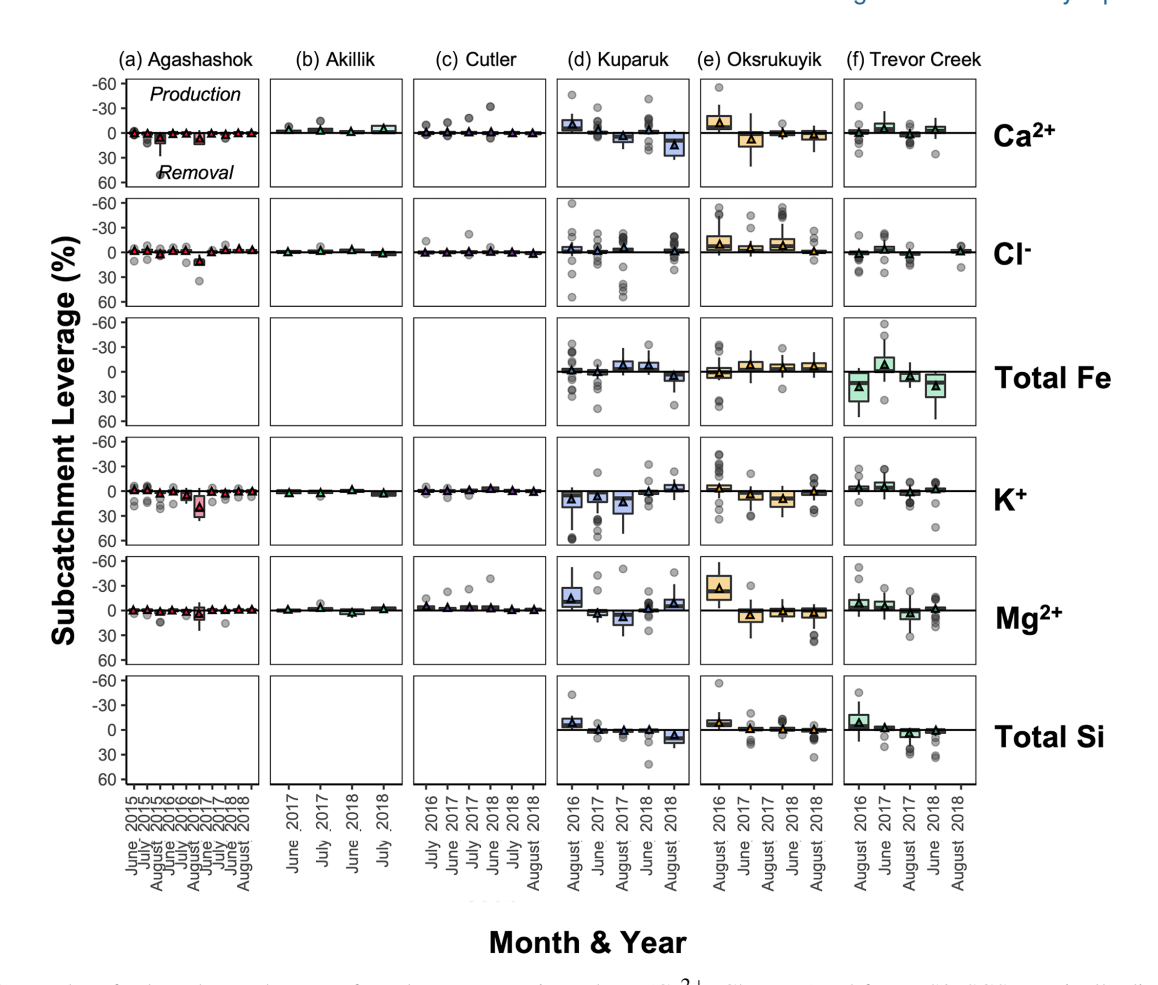


Figure 7. Boxplot of subcatchment leverage for select conservative solutes (Ca^{2+} , Cl^- , Fe (total for NPS/USGS; nominally dissolved for TFS), K^+ , Mg^{2+} , and total Si) in the (a) Agashashok River, (b) Akillik River, (c) Cutler River, (d) Kuparuk River, (e) Oksrukuyik Creek, and (f) Trevor Creek watersheds across all years and seasons sampled. Note reversed axes for ease of interpretation: negative values above the 0 line indicate production; positive values below the 0 line indicate removal. Each box encapsulates values within the lower 25th and upper 75th quartiles respectively, while the whiskers represent the minimum and maximum quartiles. Within each box, the horizontal line represents the median leverage value and the colored triangle lies at the mean. Data points outside the whiskers represent values above and below $1.5 \times$ the IQR threshold.

patches superimposed on the structure of the stream network (Abbott et al., 2018). When we plot solute concentration against subcatchment area, we find more variability water chemistry in smaller subcatchments ($< 30 \,\mathrm{km}^2$). This can be interpreted as a spatial fingerprint and is shown most clearly in Fig. 10, which displays the spatial distribution of DOC and NO₃⁻ concentrations across watersheds and sampling campaigns. Generally high concentration variability in smaller headwaters, which converges to mean watershed behavior towards the catchment outlet, holds with the conceptualizations of large rivers as chemostats (Creed et al., 2015). In the context of Arctic watersheds, these concentration-area relationships reveal consistently high DOC and low NO₃⁻ concentrations in the low-gradient tundra watersheds (Kuparuk River and Oksrukuyik Creek), despite high variability in smaller contributing subcatchments. In contrast, the alpine watershed Trevor Creek has relatively low DOC and high NO₃ concentrations, likely due to shorter and faster hydrologic flow paths and lower terrestrial biomass (Shogren et al., 2019). Overall, these findings are consistent with studies that indicate that slower, longer flow paths and productive terrestrial vegetation control carbon and nutrient transfer and mobilization in lower-gradient tundra watersheds (Shogren et al., 2019, 2021). If we assume that spatial variability in stream network water chemistry depends primarily on the extent and connectivity of upstream sources and sinks, then the patch sizes that control solute fluxes can be assessed by the spatial scale of the variance collapse (Abbott et al., 2018; Shogren et al., 2019). Across all three TFS watersheds, the generality of variance collapse at intermediate scales is indicative that subcatchment-scale patches (~ 10 -50 km²) control whether carbon and inorganic nitrogen is produced or removed at the watershed scale (Fig. 10). In addition, the consistency of the thresholds across sampling

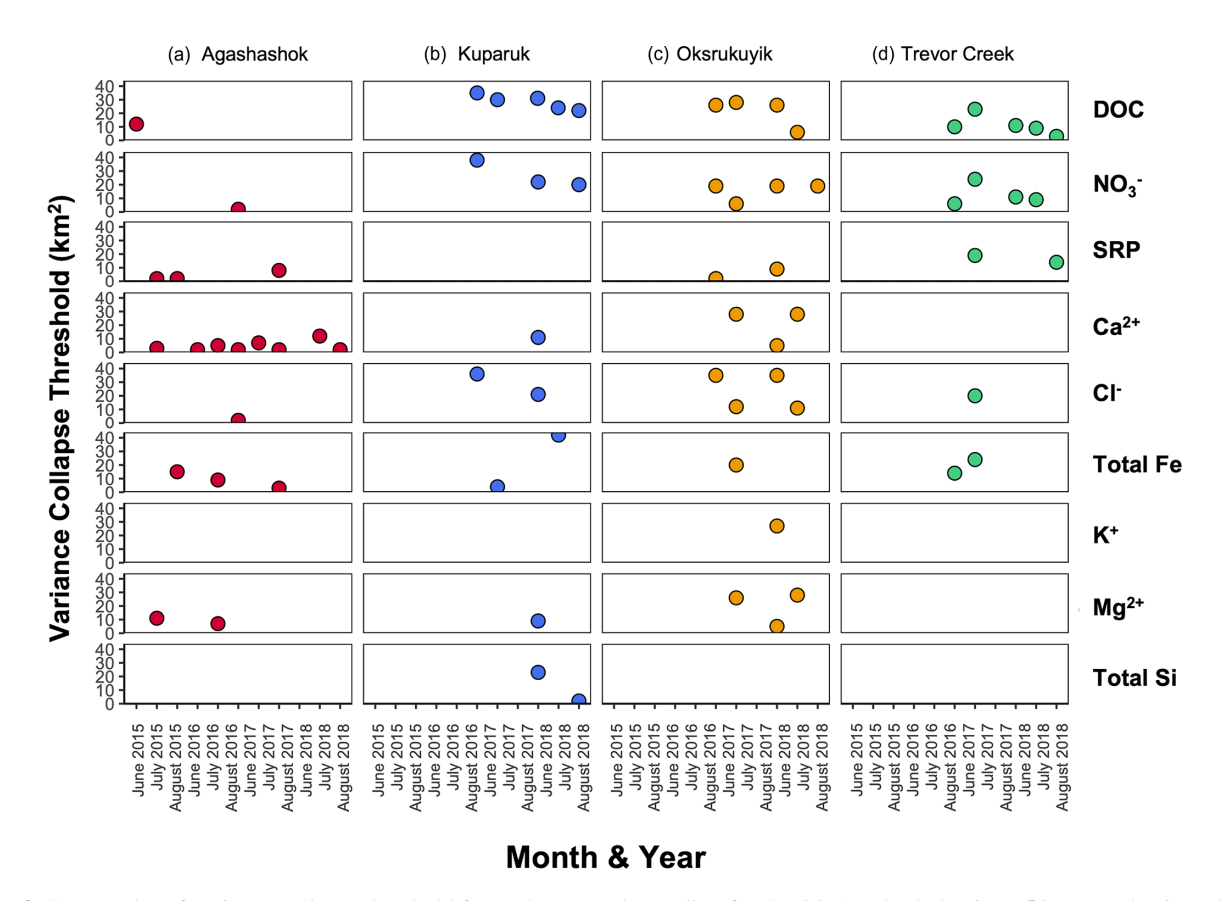


Figure 8. Scatter plot of variance collapse threshold for each repeated sampling for the (a) Agashashok River, (b) Kuparuk River, (c) Oksrukuyik Creek, and (d) Trevor Creek watersheds for select reactive (e.g., DOC, NO_3^- , and SRP) and conservative solutes (Ca^{2+} , Cl^- , Fe (total for NPS/USGS; nominally dissolved for TFS), K^+ , Mg^{2+} , and total Si). When data were not present, there was no significant collapse detected. Variance collapse thresholds are not shown for the Akillik and Cutler rivers, as these thresholds were often non-significant.

campaigns (Figs. 8 and 10) highlights the importance of capturing intermediate-scale biogeochemistry to bridge understandings from plot-level experimentation to larger more regional-scale observations (Shogren et al., 2019).

When we convert concentrations into estimates of subcatchment leverage (e.g., Figs. 6, 7, 10, and 11), patterns emerge that further contextualize the spatial distribution of DOC and NO₃⁻ concentrations. First, we can investigate whole watershed (net) behavior by calculating the mean leverage and examining the distribution of values with boxplots (as in Figs. 6 and 7). As a more specific example, mean NO₃⁻ leverage within the Kuparuk watershed (Fig. 6d, second row) were consistently above zero (note the reversed axis), revealing strong removal or retention before it reached the watershed outlet, which is consistent with high biotic N demand. Within this same watershed, DOC leverage values were often at or just above the zero line (Fig. 6d, first row), representing primarily conservative transport of DOC (i.e., no net production or uptake). Within the lake-influenced Oksrukuyik watershed, NO₃⁻ leverage values were more variable (i.e., leverage above and below the zero line; Fig. 6e, second row), implying a combination of removal and production mechanisms acting across the watershed network. When visualized as net behavior, the watershed and season-dependent directionality of net leverage patterns are congruent with emerging evidence that landscape template exerts strong control on biogeochemical signals in Arctic rivers (Vonk et al., 2019; Tank et al., 2020; Shogren et al., 2021). As a complement to the first approach, we can additionally examine individual subcatchment leverage values to reveal the effect of each contribution on what we observe at the watershed outlet. This can be interpreted similarly to statistical leverage, where one or more points may exert high influence on a linear regression.

Across all TFS watersheds, there are a few select subcatchments that contribute disproportionately to DOC fluxes, while the more variable patterns for NO₃⁻ suggest additional spatial and seasonal controls (Fig. 11). For example, patterns in the Kuparuk River and Oksrukuyik Creek (Fig. 11a and b) could be interpreted to mean that DOC is transported conservatively in lower-gradient landscapes, while lateral fluxes of NO₃⁻ are more tightly controlled by biotic demand (Harms et al., 2016; Khosh et al., 2017; Connolly et al., 2018; Kendrick et al., 2018; Iannucci et al., 2021). Across solutes

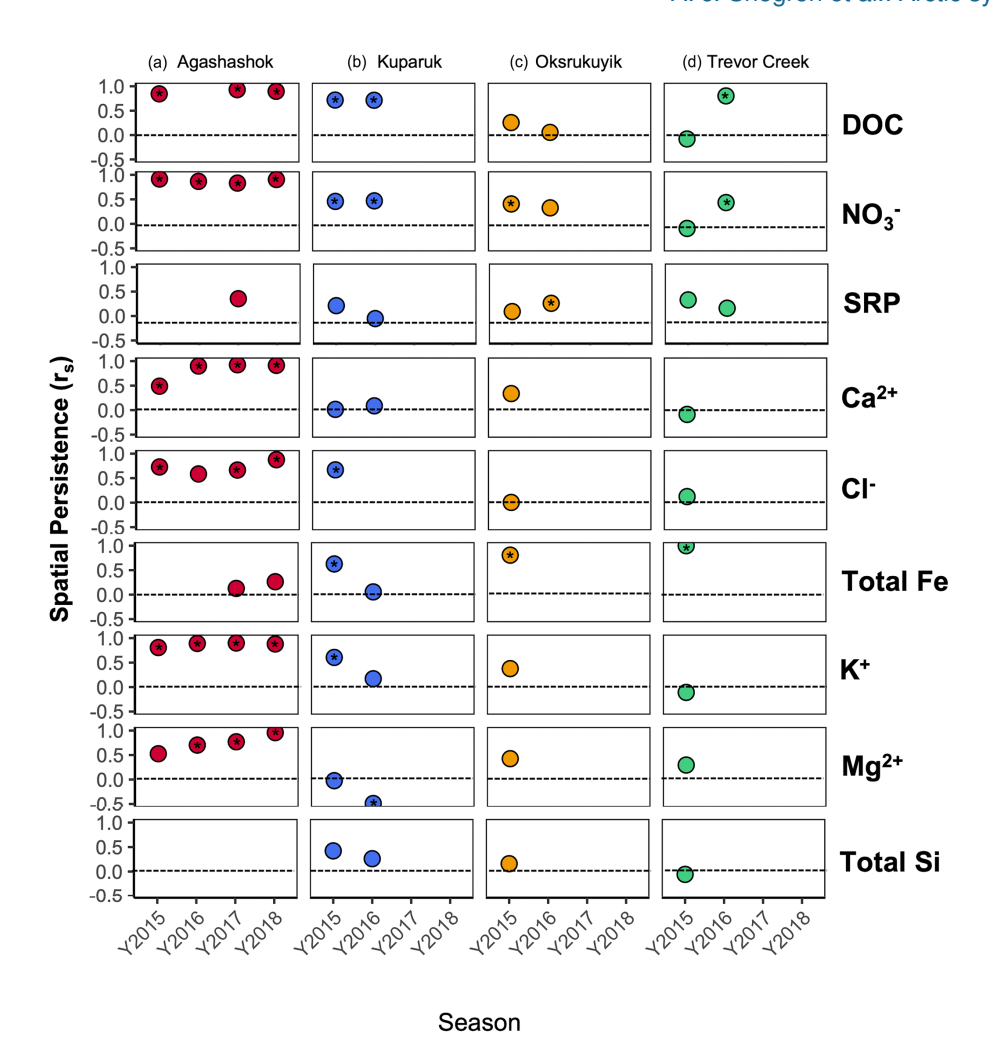


Figure 9. Scatter plot of spatial stability (r_s) for each repeated sampling for the **(a)** Agashashok, **(b)** Kuparuk River, **(c)** Oksrukuyik Creek, and **(d)** Trevor Creek watersheds for select reactive (e.g., DOC, NO₃⁻, and SRP) and conservative solutes (Ca²⁺, Cl⁻, Fe (total for NPS/USGS; nominally dissolved for TFS), K⁺, Mg²⁺, and total Si). When data were not present, there is no spatial stability reported. When Spearman's rank correlation (r_s) is significant, this is denoted by an asterisk (*) within the point.

and watersheds, the information gleaned from the leverage metric is useful in several ways. First, subcatchment leverages allow for the direct identification of watershed areas that are disproportionately driving carbon and nutrient exports. For any chosen solute or suite of materials, sites identified as "high leverage" indicate strong source/sink behavior, which could be (1) validated with regular field observations that relate riparian or terrestrial conditions with empirical measurements of water chemistry, (2) selected for further study designed to identify the abiotic and biotic mechanisms that drive patterns of riverine chemistry, and/or (3) identified as non-representative sites relative to proximal subcatchments of similar size and terrestrial characteristics. Relatedly, estimating subcatchment leverage enables researchers to identify sites that are representative of watershed-scale behavior, which could be used to more effectively scale biogeochemical dynamics in Arctic rivers relative to outlying subcatchments (Kicklighter et al., 2013; Pinay et al., 2015; Aguilera et al., 2013).

Finally, the application of the simple spatial persistence metric can help researchers determine whether a sampling location is behaving consistently, or if solute contributions are moving in space across sampling events (Abbott et al., 2018; Dupas et al., 2019). In the context of work in remote watersheds, the ability for researchers to identify both stable and unstable processes presents an exciting opportunity to ask questions about the consistency of subcatchment contributions and optimize sampling or experimental design. For example, DOC concentrations are generally spatially stable between early and late sampling events ($r_s > 0.50$), particularly in the Kuparuk River and Trevor Creek watersheds (Fig. 9). In these landscapes, a high rank correlation indicates that repeated sampling of the same location will result in a similar spatial distribution of concentrations. While

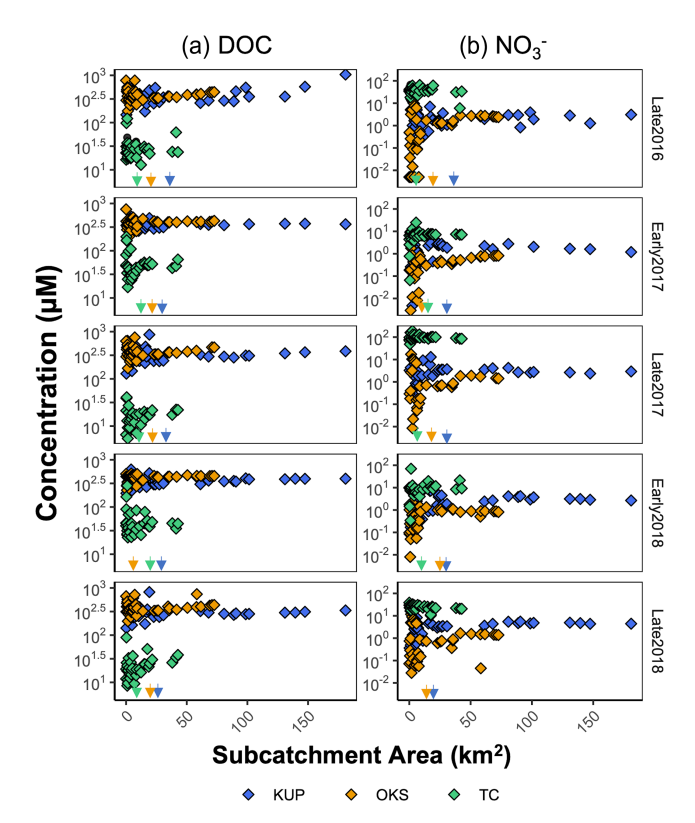


Figure 10. Scatter plot of log-scale (a) DOC and (b) NO_3^- concentrations (μ M) across subcatchment area (km²) or each repeated sampling in the Kuparuk River (blue points), Oksrukuyik Creek (orange points), and Trevor Creek (green points) watersheds. Significant variance collapse thresholds are represented by a colored arrow.

sampling repeatedly in the early and late seasons may reveal increases or decreases in solute concentrations (Shogren et al., 2019), the high degree of relatedness indicates that these patterns will be maintained across the watershed network. However, the low persistence ($r_{\rm s} < 0.50$) for DOC in the Oksrukuyik Creek watersheds signifies substantial spatial shifts across the early and late thaw season (Shogren et al., 2019). While there was variability in the persistence across watersheds and solutes, the stability metric can be used by future researchers to identify whether sampling the same location repeatedly does or does not represent the spatial dynamics across sampling events.

4 Data availability

The data from the NPS/USGS are available at https://doi.org/10.5066/P9SBK2DZ (O'Donnell et al., 2021). Data from TFS are stored at the Environmental Data Center data repository (https://doi.org/10.6073/pasta/258a44fb9055163dd4dd4371b9dce945, Abbott, 2021).

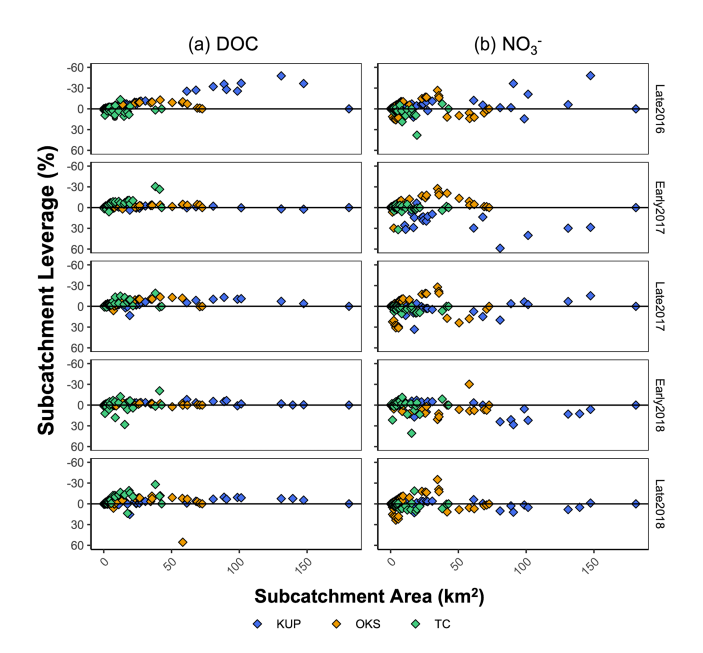


Figure 11. Scatter plot of **(a)** DOC and **(b)** NO₃⁻ leverages across subcatchment area (km²) or each repeated sampling in the Kuparuk River (blue points), Oksrukuyik Creek (orange points), and Trevor Creek (green points) watersheds. Note reversed axes for ease of interpretation: negative values above the 0 line indicate production; positive values below the 0 line indicate removal.

5 Conclusions

With this work, we provide a detailed characterization of physical, chemical, and biological parameters that are essential to using river network chemistry to infer ecosystem-level carbon and nutrient balance. We apply novel metrics to these data that describe the spatiotemporal patterns of watershed biogeochemistry in six permafrost-underlain Arctic watersheds. These data represent a high-resolution and temporally replicated river chemistry dataset from understudied permafrost-dominated regions. Combining these measures with remotely sensed data, plot-level experiments, and numerical models could advance our understanding of permafrost ecosystems in the face of climate change and other disturbance.

Author contributions. All co-authors participated in the field collection, laboratory analysis, and/or curation of the dataset and contributed to writing and/or editing this paper. AJS was primarily responsible for writing this paper and assembly of the archival database.

Competing interests. The contact author has declared that neither they nor their co-authors have any competing interests.

Disclaimer. Publisher's note: Copernicus Publications remains neutral with regard to jurisdictional claims in published maps and institutional affiliations.

Special issue statement. This article is part of the special issue "Extreme environment datasets for the three poles". It is not associated with a conference.

Acknowledgements. Data and facilities were provided by the Arctic LTER at TFS, NPS, and USFS. The authors gratefully acknowledge the Arctic LTER, TFS staff, and CH2M HILL Polar Services for assistance in support of this work. The authors also thank the National Park Service's Western Arctic National Parklands in Kotzebue, Alaska, for assisting with logistics and permitting. DEMs were provided by the Polar Geospatial Center under NSF-OPP awards 1043681, 1559691, and 1542736.

The authors would also like to acknowledge their funding support: AJS (NSF-DBI-1906381, NSF-OPP-1916567), JPZ and TW (NSF-EAR-1846855, NSF-OPP-1916567), BWA (NSF-OPP-1916565), WBB (NSF-OPP-1916576, NSF DEB-1637459), and FI and AM (NSF DEB-1637459). This work was supported by the Changing Arctic Ecosystems Initiative of the Wildlife Program of the USGS Ecosystems Mission Area. Additional support was provided by the NPS Arctic Inventory and Monitoring Network. Any use of trade, firm, or product names is for descriptive purposes only and does not imply endorsement by the U.S. Government.

Financial support. This research has been supported by the National Science Foundation (grant nos. 1906381, 1637459, 1916567, 1916576, 1916565, and 1846855).

Review statement. This paper was edited by Min Feng and reviewed by two anonymous referees.

References

- Abbott, B.: Repeated synoptic watershed chemistry from three watersheds near Toolik Field Station, Alaska, summer 2016-2018, ver 2, Environmental Data Initiative [data set], https://doi.org/10.6073/pasta/258a44fb9055163dd4dd4371b9dce945, 2021.
- Abbott, B. W., Jones, J. B., Godsey, S. E., Larouche, J. R., and Bowden, W. B.: Patterns and persistence of hydrologic carbon and nutrient export from collapsing upland permafrost, Biogeosciences, 12, 3725–3740, https://doi.org/10.5194/bg-12-3725-2015, 2015.
- Abbott, B. W., Baranov, V., Mendoza-Lera, C., Nikolakopoulou, M., Harjung, A., Kolbe, T., Balasubramanian, M. N., Vaessen, T. N., Ciocca, F., Campeau, A., Wallin, M. B., Romeijn, P., Antonelli, M., Gonçalves, J., Datry, T., Laverman, A. M., de Dreuzy, J.-R., Hannah, D. M., Krause, S., Oldham, C., and Pinay, G.: Using multi-tracer inference to move beyond single-catchment ecohydrology, Earth-Sci. Rev., 160, 19–42, https://doi.org/10.1016/j.earscirev.2016.06.014, 2016.

- Abbott, B. W., Pinay, G., and Burt, T. P.: Protecting Water Resources Through a Focus on Headwater Streams, EOS, 98, EO076897, https://doi.org/10.1029/2017EO076897, 2017.
- Abbott, B. W., Gruau, G., Zarnetske, J. P., Moatar, F., Barbe, L., Thomas, Z., Fovet, O., Kolbe, T., Gu, S., Pierson-Wickmann, A.-C., Davy, P., and Pinay, G.: Unexpected spatial stability of water chemistry in headwater stream networks, Ecol. Lett., 21, 296– 308, https://doi.org/10.1111/ele.12897, 2018.
- Abbott, B. W., Rocha, A. V., Shogren, A., Zarnetske, J. P., Iannucci, F., Bowden, W. B., Bratsman, S. P., Patch, L., Watts, R., Fulweber, R., Frei, R. J., Huebner, A. M., Ludwig, S. M., Carling, G. T., and O'Donnell, J. A.: Tundra wildfire triggers sustained lateral nutrient loss in Alaskan Arctic, Glob. Change Biol., 27, 1408–1430, https://doi.org/10.1111/gcb.15507, 2021.
- Aguilera, R., Marcé, R., and Sabater, S.: Modeling nutrient retention at the watershed scale: Does small stream research apply to the whole river network?: Nutrient retention in impaired rivers, J. Geophys. Res.-Biogeosci., 118, 728–740, https://doi.org/10.1002/jgrg.20062, 2013.
- Appling, A. P., Hall, R. O., Yackulic, C. B., and Arroita, M.: Overcoming Equifinality: Leveraging Long Time Series for Stream Metabolism Estimation, J. Geophys. Res.-Biogeosci., 123, 624–645, https://doi.org/10.1002/2017JG004140, 2018.
- Asano, Y., Uchida, T., Mimasu, Y., and Ohte, N.: Spatial patterns of stream solute concentrations in a steep mountainous catchment with a homogeneous landscape, Water Resour. Res., 45, W10432, https://doi.org/10.1029/2008WR007466, 2009.
- Bernhardt, E. S., Blaszczak, J. R., Ficken, C. D., Fork, M. L., Kaiser, K. E., and Seybold, E. C.: Control Points in Ecosystems: Moving Beyond the Hot Spot Hot Moment Concept, Ecosystems, 20, 665–682, https://doi.org/10.1007/s10021-016-0103-y, 2017.
- W. B.: CSASN Channel Nutrients Bowden. from 2010 to 2012 in I8 Inlet, I8 Outlet, Peat Inlet and Kuparuk Rivers, Environmental Data Initiative (EDI) Portal [data set], https://doi.org/10.6073/pasta/ d19adb5a8fe01f67806e5afccf283b52, 2013.
- Bring, A., Fedorova, I., Dibike, Y., Hinzman, L., Mård, J., Mernild, S. H., Prowse, T., Semenova, O., Stuefer, S. L., and Woo, M.-K.: Arctic terrestrial hydrology: A synthesis of processes, regional effects, and research challenges, J. Geophys. Res.-Biogeosci., 121, 621–649, https://doi.org/10.1002/2015JG003131, 2016.
- Burns, D. A., Pellerin, B. A., Miller, M. P., Capel, P. D., Tesoriero, A. J., and Duncan, J. M.: Monitoring the riverine pulse: Applying high-frequency nitrate data to advance integrative understanding of biogeochemical and hydrological processes, WIREs Water, 6, e1348, https://doi.org/10.1002/wat2.1348, 2019.
- Burt, T. P. and Pinay, G.: Linking hydrology and biogeochemistry in complex landscapes, Prog. Phys. Geog., 29, 297–316, https://doi.org/10.1191/0309133305pp450ra, 2005.
- Byrne, P., Runkel, R. L., and Walton-Day, K.: Synoptic sampling and principal components analysis to identify sources of water and metals to an acid mine drainage stream, Environ. Sci. Pollut. Res., 24, 17220–17240, https://doi.org/10.1007/s11356-017-9038-x, 2017.
- Collier, N., Hoffman, F. M., Lawrence, D. M., Keppel-Aleks, G., Koven, C. D., Riley, W. J., Mu, M., and Randerson, J. T.: The International Land Model Benchmarking (ILAMB) System: Design, Theory, and Implementation, J. Adv. Model. Earth Sy., 10, 2731–2754, https://doi.org/10.1029/2018MS001354, 2018.

- Connolly, C. T., Khosh, M. S., Burkart, G. A., Douglas, T. A., Holmes, R. M., Jacobson, A. D., Tank, S. E., and McClelland, J. W.: Watershed slope as a predictor of fluvial dissolved organic matter and nitrate concentrations across geographical space and catchment size in the Arctic, Environ. Res. Lett., 13, 104015– 104015, https://doi.org/10.1088/1748-9326/aae35d, 2018.
- Covino, T.: Hydrologic connectivity as a framework for understanding biogeochemical flux through watersheds and along fluvial networks, Geomorphology, 277, 133–144, https://doi.org/10.1016/j.geomorph.2016.09.030, 2017.
- Creed, I. F., McKnight, D. M., Pellerin, B. A., Green, M. B., Bergamaschi, B. A., Aiken, G. R., Burns, D. A., Findlay, S. E. G., Shanley, J. B., Striegl, R. G., Aulenbach, B. T., Clow, D. W., Laudon, H., McGlynn, B. L., McGuire, K. J., Smith, R. A., and Stackpoole, S. M.: The river as a chemostat: fresh perspectives on dissolved organic matter flowing down the river continuum, Can. J. Fish. Aquat. Sci., 72, 1272–1285, https://doi.org/10.1139/cjfas-2014-0400, 2015.
- Docherty, C. L., Riis, T., Hannah, D. M., Rosenhøj Leth, S., and Milner, A. M.: Nutrient uptake controls and limitation dynamics in north-east Greenland streams, Polar Res, 37, 1440107, https://doi.org/10.1080/17518369.2018.1440107, 2018.
- Dupas, R., Minaudo, C., and Abbott, B. W.: Stability of spatial patterns in water chemistry across temperate ecoregions, Environ. Res. Lett., 14, 074015, https://doi.org/10.1088/1748-9326/ab24f4, 2019.
- ESRI: ArcGIS Desktop: Release 10.4.1, Environmental Systems Research Institute, Redlands, CA, 2016.
- Farquharson, L. M., Romanovsky, V. E., Cable, W. L., Walker, D. A., Kokelj, S., and Nicolsky, D.: Climate change drives widespread and rapid thermokarst development in very cold permafrost in the Canadian High Arctic, Geophys. Res. Lett., Geophys. Res. Lett., 46, 6681–6689, https://doi.org/10.1029/2019GL082187, 2019.
- Frei, R. J., Abbott, B. W., Dupas, R., Gu, S., Gruau, G., Thomas, Z., Kolbe, T., Aquilina, L., Labasque, T., Laverman, A., Fovet, O., Moatar, F., and Pinay, G.: Predicting Nutrient Incontinence in the Anthropocene at Watershed Scales, Front. Environ. Sci., 7, 200, https://doi.org/10.3389/fenvs.2019.00200, 2020.
- Gao, T., Zhang, Y., Kang, S., Abbott, B. W., Wang, X., Zhang, T., Yi, S., and Gustafsson, O.: Accelerating permafrost collapse on the Eastern Tibetan Plateau, Environ. Res. Lett., 16 054023, https://doi.org/10.1088/1748-9326/abf7f0, 2021.
- Gardner, K. K. and McGlynn, B. L.: Seasonality in spatial variability and influence of land use/land cover and watershed characteristics on stream water nitrate concentrations in a developing watershed in the Rocky Mountain West, Water Resour. Res., 45, W08411, https://doi.org/10.1029/2008WR007029, 2009.
- Gu, S., Casquin, A., Dupas, R., Abbott, B. W., Petitjean, P., Durand, P., and Gruau, G.: Spatial Persistence of Water Chemistry Patterns Across Flow Conditions in a Mesoscale Agricultural Catchment, Water Resour. Res., 57, e2020WR029053, https://doi.org/10.1029/2020WR029053, 2021.
- Hansen, A. M., Kraus, T. E. C., Pellerin, B. A., Fleck, J. A., Downing, B. D., and Bergamashi, B. A.: Optical properties of dissolved organic matter (DOM): effects of biological and photolytic degradation, Limnol. Oceanogr., 61, 1015–1032, https://doi.org/10.1002/lno.10270, 2016.

- Harms, T. K., Edmonds, J. W., Genet, H., Creed, I. F., Aldred, D., Balser, A., and Jones, J. B.: Catchment influence on nitrate and dissolved organic matter in Alaskan streams across a latitudinal gradient, J. Geophys. Res.-Biogeosci., 121, 350–369, https://doi.org/10.1002/2015JG003201, 2016.
- Helms, J. R., Stubbins, A., Ritchie, J. D., Minor, E. C., Kieber, D. J., and Mopper, K.: Adsorption spectral slopes and slope ratios as indicators of molecular weight, source, and photobleaching of chromophoric dissolved organic matter, Limnol. Oceanogr., 53, 955–969, https://doi.org/10.4319/lo.2008.53.3.0955, 2008.
- Helton, A. M., Poole, G. C., Payn, R. A., Izurieta, C., and Stanford, J. A.: Scaling flow path processes to fluvial landscapes: An integrated field and model assessment of temperature and dissolved oxygen dynamics in a river-floodplain-aquifer system, J. Geophys. Res., 117, G00N14, https://doi.org/10.1029/2012JG002025, 2012.
- Hobbie, J. E. and Kling, G. W. (Eds.): Alaska's Changing Arctic, Oxford University Press, New York, NY, USA, https://doi.org/10.1093/acprof:osobl/9780199860401.001.0001, 2014.
- Hoffman, F. M., Kumar, J., Mills, R. T., and Hargrove, W. W.: Representativeness-based sampling network design for the State of Alaska, Landscape Ecol., 28, 1567–1586, 2013.
- Iannucci, F. M., Beneš, J., Medvedeff, A., and Bowden, W. B.: Biogeochemical responses over 37 years to manipulation of phosphorus concentrations in an Arctic river: The Upper Kuparuk River Experiment, Hydrol. Process., 35, e14075, https://doi.org/10.1002/hyp.14075, 2021.
- Kareiva, P. and Andersen, M.: Spatial Aspects of Species Interactions: the Wedding of Models and Experiments, Springer, Berlin, Heidelberg, 35–50, https://doi.org/10.1007/978-3-642-85936-6_4, 1988.
- Karlsen, R. H., Grabs, T., Bishop, K., Buffam, I., Laudon, H., and Seibert, J.: Landscape controls on spatiotemporal discharge variability in a boreal catchment, Water Resour. Res., 52, 6541–6556, https://doi.org/10.1002/2016WR019186, 2016.
- Keller, K., Blum, J. D., and Kling, G. W.: Geochemistry of soils and streams on surfaces of varying ages in arctic Alaska, Arct. Antarct. Alp. Res., 39, 84–98, https://doi.org/10.1657/1523-0430(2007)39[84:GOSASO]2.0.CO;2, 2007.
- Kendrick, M. R., Huryn, A. D., Bowden, W. B., Deegan, L. A., Findlay, R. H., Hershey, A. E., Peterson, B. J., Beneš, J. P., and Schuett, E. B.: Linking permafrost thaw to shifting biogeochemistry and food web resources in an arctic river, Glob. Change Biol., 24, 5738–5750, https://doi.org/10.1111/gcb.14448, 2018.
- Khamis, K., Blaen, P. J., Comer-Warner, S., Hannah, D. M., MacKenzie, A. R., and Krause, S.: High-Frequency Monitoring Reveals Multiple Frequencies of Nitrogen and Carbon Mass Balance Dynamics in a Headwater Stream, Front. Water, 3, 668924, https://doi.org/10.3389/frwa.2021.668924, 2021.
- Khosh, M. S., McClelland, J. W., Jacobson, A. D., Douglas, T. A., Barker, A. J., and Lehn, G. O.: Seasonality of dissolved nitrogen from spring melt to fall freezeup in Alaskan Arctic tundra and mountain streams, J. Geophys. Res.-Biogeosci., 122, 1718–1737, https://doi.org/10.1002/2016JG003377, 2017.
- Kicklighter, D. W., Hayes, D. J., McClelland, J. W., Peterson, B. J., McGuire, A. D., and Melillo, J. M.: Insights and issues with simulating terrestrial DOC loading of Arctic river networks, Ecol. Appl., 23, 1817–1836, https://doi.org/10.1890/11-1050.1, 2013.

- Killick, R. and Eckley, I. A.: changepoint: An R Package for Changepoint Analysis, J. Stat. Softw., 58, 1–19, 2014.
- Kling, G. W., Kipphut, G. W., Miller, M. M., and O'Brien, W. J.: Integration of lakes and streams in a landscape perspective: the importance of material processing on spatial patterns and temporal coherence, Freshwater Biol., 43, 477–497, https://doi.org/10.1046/j.1365-2427.2000.00515.x, 2000.
- Kolbe, T., de Dreuzy, J.-R., Abbott, B. W., Aquilina, L., Babey, T., Green, C. T., Fleckenstein, J. H., Labasque, T., Laverman, A. M., Marçais, J., Peiffer, S., Thomas, Z., and Pinay, G.: Stratification of reactivity determines nitrate removal in groundwater, P. Natl. Acad. Sci. USA, 116, 2494–2499, https://doi.org/10.1073/pnas.1816892116, 2019.
- Koven, C. D., Lawrence, D. M., and Riley, W. J.: Permafrost carbon–climate feedback is sensitive to deep soil carbon decomposability but not deep soil nitrogen dynamics, P. Natl. Acad. Sci. USA, 112, 3752–3757, https://doi.org/10.1073/pnas.1415123112, 2015.
- Lamhonwah, D., Lafreniere, M. J., Lamoureux, S. F., and Wolfe, B. B.: Evaluating the hydrological and hydrochemical responses of a High Arctic catchment during an exceptionally warm summer, Hydrol. Process., 31, 2296–2313, https://doi.org/10.1002/hyp.11191, 2017.
- Laudon, H., Spence, C., Buttle, J., Carey, S. K., McDonnell, J. J., McNamara, J. P., Soulsby, C., and Tetzlaff, D.: Save northern high-latitude catchments, Nat. Geosci., 10, 324–325, https://doi.org/10.1038/ngeo2947, 2017.
- Lecher, A.: Groundwater Discharge in the Arctic: A Review of Studies and Implications for Biogeochemistry, Hydrology , 4, 41, https://doi.org/10.3390/hydrology4030041, 2017.
- McClelland, J. W., Déry, S. J., Peterson, B. J., Holmes, R. M., and Wood, E. F.: A pan-arctic evaluation of changes in river discharge during the latter half of the 20th century, Geophys. Res. Lett., 33, L06715, https://doi.org/10.1029/2006GL025753, 2006.
- McClelland, J. W., Stieglitz, M., Pan, F., Holmes, R. M., and Peterson, B. J.: Recent changes in nitrate and dissolved organic carbon export from the upper Kuparuk River, North Slope, Alaska, J. Geophys. Res., 112, G04S60, https://doi.org/10.1029/2006JG000371, 2007.
- McDonnell, J. J., Sivapalan, M., Vaché, K., Dunn, S., Grant, G., Haggerty, R., Hinz, C., Hooper, R., Kirchner, J. W., Roderick, M. L., Selker, J., and Weiler, M.: Moving beyond heterogeneity and process complexity: A new vision for watershed hydrology, Water Resour. Res., 43, W07301, https://doi.org/10.1029/2006WR005467, 2007.
- McGuire, K. J., Torgersen, C. E., Likens, G. E., Buso, D. C., Lowe, W. H., and Bailey, S. W.: Network analysis reveals multiscale controls on streamwater chemistry, P. Natl. Acad. Sci. USA, 111, 7030–7035, https://doi.org/10.1073/pnas.1404820111, 2014.
- Moatar, F., Abbott, B. W., Minaudo, C., Curie, F., and Pinay, G.: Elemental properties, hydrology, and biology interact to shape concentration-discharge curves for carbon, nutrients, sediment, and major ions, Water Resour. Res., 53, 1270–1287, https://doi.org/10.1002/2016WR019635, 2017.
- Mu, C., Abbott, B. W., Norris, A. J., Mu, M., Fan, C., Chen, X., Jia, L., Yang, R., Zhang, T., Wang, K., Peng, X., Wu, Q., Guggenberger, G., and Wu, X.: The status and stability of permafrost carbon on the Tibetan Plateau, Earth-Sci. Rev., 211, 103433, https://doi.org/10.1016/j.earscirev.2020.103433, 2020.

- Muller, S., Walker, D. A., and Jorgenson, M. T.: Land Cover and Ecosystem Map Collection for Northern Alaska, ORNL DAAC [data set], Oak Ridge, Tennessee, USA, https://doi.org/10.3334/ORNLDAAC/1359, 2018.
- NASA/METI/AIST/Japan Space Systems and US/Japan ASTER Science Team: ASTER Global Digital Elevation Model [data set], https://doi.org/10.5067/ASTER/ASTGTM.002, 2009.
- Newman, E. A., Kennedy, M. C., Falk, D. A., and McKenzie, D.: Scaling and Complexity in Landscape Ecology, Front. Ecol. Evol., 7, 293, https://doi.org/10.3389/fevo.2019.00293, 2019.
- O'Donnell, J. A., Aiken, G. R., Swanson, D. K., Panda, S., Butler, K. D., and Baltensperger, A. P.: Dissolved organic matter composition of Arctic rivers: Linking permafrost and parent material to riverine carbon, Global Biogeochem. Cy., 30, 1811–1826, https://doi.org/10.1002/2016GB005482, 2016.
- O'Donnell, J. A., Carey, M. P., Koch, J. C., Xu, X., Poulin, B. A., Walker, J., and Zimmerman, C. E.: Permafrost Hydrology Drives the Assimilation of Old Carbon by Stream Food Webs in the Arctic, Ecosystems, 23, 435–453, https://doi.org/10.1007/s10021-019-00413-6, 2020.
- O'Donnell, J. A., Koch, J. C., Carey, M. P., and Poulin, B. A.: Stream and river chemistry in watersheds of northwestern Alaska, 2015-2019, U.S. Geological Survey, USGS Alaska Science Center [data set], https://doi.org/10.5066/P9SBK2DZ, 2021
- Panda, S., Romanovsky, V., and Marchenk, S.: High-resolution permafrost modeling in the Arctic Network National Parks, Preserves, & Monuments, National Park Service, Fort Collins, Colorado, 2016.
- Peterson, B. J., Deegan, L., Helfrich, J., Hobbie, J. E., Hullar, M., Moller, B., Ford, T. E., Hershey, A., Hiltner, A., Kipphut, G., Lock, M. A., Fiebig, D. M., McKinley, V., Miller, M. C., Vestal, J. R., Ventullo, R., and Volk, G.: Biological Responses of a Tundra River to Fertilization, Ecology, 74, 653–672, https://doi.org/10.2307/1940794, 1993.
- Pinay, G., Peiffer, S., De Dreuzy, J.-R., Krause, S., Hannah, D. M., Fleckenstein, J. H., Sebilo, M., Bishop, K., and Hubert-Moy, L.: Upscaling Nitrogen Removal Capacity from Local Hotspots to Low Stream Orders' Drainage Basins, Ecosystems, 18, 1101–1120, https://doi.org/10.1007/s10021-015-9878-5, 2015.
- Porter, C., Morin, P., Howat, I., Noh, M.-J., Bates, B., Peterman, K., Keesey, S., Schlenk, M., Gardiner, J., Tomko, K., Willis, M., Kelleher, C., Cloutier, M., Husby, E., Foga, S., Nakumura, H., Platson, M., Wethington, M., Williamson, C., Bauer, G., Enos, J., Arnold, G., William, K., Becker, P., Doshi, A., D'Souza, C., Cummens, P., Laurier, F., and Bojezen, M.: Arctic DEM, Polar Geospatial Center [data set], https://doi.org/10.7910/DVN/OHHUKH, 2018.
- Prager, C. M., Naeem, S., Boelman, N. T., Eitel, J. U. H. H., Greaves, H. E., Heskel, M. A., Magney, T. S., Menge, D. N. L., Vierling, L. A., and Griffin, K. L.: A gradient of nutrient enrichment reveals nonlinear impacts of fertilization on Arctic plant diversity and ecosystem function, Ecol Evol., 7, 2449–2460, https://doi.org/10.1002/ece3.2863, 2017.
- Rodríguez-Cardona, B. M., Coble, A. A., Wymore, A. S., Kolosov,
 R., Podgorski, D. C., Zito, P., Spencer, R. G. M., Prokushkin,
 A. S., and McDowell, W. H.: Wildfires lead to decreased carbon
 and increased nitrogen concentrations in upland arctic streams,

- Sci. Rep., 10, 8722, https://doi.org/10.1038/s41598-020-65520-0.2020
- Ruhala, S. S. and Zarnetske, J. P.: Using in-situ optical sensors to study dissolved organic carbon dynamics of streams and watersheds: A review, Sci. Total Environ., 575, 713–723, https://doi.org/10.1016/j.scitotenv.2016.09.113, 2017.
- Schuur, E. A. G., McGuire, A. D., Schädel, C., Grosse, G., Harden, J. W., Hayes, D. J., Hugelius, G., Koven, C. D., Kuhry, P., Lawrence, D. M., Natali, S. M., Olefeldt, D., Romanovsky, V. E., Schaefer, K., Turetsky, M. R., Treat, C. C., and Vonk, J. E.: Climate change and the permafrost carbon feedback, Nature, 520, 171–179, https://doi.org/10.1038/nature14338, 2015.
- Shiklomanov, A. N., Bradley, B. A., Dahlin, K. M., Fox, A. M., Gough, C. M., Hoffman, F. M., Middleton, E. M., Serbin, S. P., Smallman, L., and Smith, W. K.: Enhancing global change experiments through integration of remote-sensing techniques, Front. Ecol. Environ., 17, 215–224, https://doi.org/10.1002/fee.2031, 2019.
- Shogren, A. J., Zarnetske, J. P., Abbott, B. W., Iannucci, F., Frei, R. J., Griffin, N. A., and Bowden, W. B.: Revealing biogeochemical signatures of Arctic landscapes with river chemistry, Sci. Rep., 9, 12894, https://doi.org/10.1038/s41598-019-49296-6, 2019.
- Shogren, A. J., Zarnetske, J. P., Abbott, B. W., Iannucci, F., and Bowden, W. B.: We cannot shrug off the shoulder seasons: Addressing knowledge and data gaps in an Arctic Headwater, Environ. Res. Lett., 15 104027, https://doi.org/10.1088/1748-9326/ab9d3c, 2020.
- Shogren, A. J., Zarnetske, J. P., Abbott, B. W., Iannucci, F., Medvedeff, A., Cairns, S., Duda, M. J., and Bowden, W. B.: Arctic concentration–discharge relationships for dissolved organic carbon and nitrate vary with landscape and season, Limnol. Oceanogr., 66, S197–S215, https://doi.org/10.1002/lno.11682, 2021.
- Sivapalan, M.: Process complexity at hillslope scale, process simplicity at the watershed scale: is there a connection?, Hydrol. Process., 17, 1037–1041, https://doi.org/10.1002/hyp.5109, 2003.
- Sjöberg, Y., Jan, A., Painter, S. L., Coon, E. T., Carey, M. P., O'Donnell, J. A., and Koch, J. C.: Permafrost Promotes Shallow Groundwater Flow and Warmer Headwater Streams, Water Resour. Res., 57, e2020WR027463, https://doi.org/10.1029/2020WR027463, 2021.
- Slavik, K., Peterson, B. J., Deegan, L. A., Bowden, W. B., Hershey, A. E., and Hobbie, J. E.: Long-Term Responses of the Kuparuk River Ecosystem to Phosphorus Fertilization, Ecology, 85, 939– 954, https://doi.org/10.1890/02-4039, 2004.
- Suarez, F., Binkley, D., Kaye, M. W., and Stottlemyer, R.: Expansion of forest stands into tundra in the Noatak National Preserve, northwest Alaska, Écoscience, 6, 465–470, https://doi.org/10.1080/11956860.1999.11682538, 1999.
- Tank, S. E., Striegl, R. G., McClelland, J. W., and Kokelj, S. V.: Multi-decadal increases in dissolved organic carbon and alkalinity flux from the Mackenzie drainage basin to the Arctic Ocean, Environ. Res. Lett., 11, 054015, https://doi.org/10.1088/1748-9326/11/5/054015, 2016.
- Tank, S. E., Vonk, J. E., Walvoord, M. A., McClelland, J. W., Laurion, I., and Abbott, B. W.: Landscape matters: Predicting the biogeochemical effects of permafrost thaw on aquatic networks with a state factor approach, Permafrost Periglac., 31, 358–370, https://doi.org/10.1002/ppp.2057, 2020.

- Temnerud, J. and Bishop, K.: Spatial Variation of Streamwater Chemistry in Two Swedish Boreal Catchments: Implications for Environmental Assessment, Environ. Sci. Technol., 39, 1463– 1469, https://doi.org/10.1021/ES040045Q, 2005.
- Temnerud, J., Fölster, J., Buffam, I., Laudon, H., Erlandsson, M., and Bishop, K.: Can the distribution of headwater stream chemistry be predicted from downstream observations?, Hydrol. Process., 24, 2269–2276, https://doi.org/10.1002/hyp.7615, 2010.
- Terry, N., Grunewald, E., Briggs, M., Gooseff, M., Huryn, A. D., Kass, M. A., Tape, K. D., Hendrickson, P., and Lane, J. W.: Seasonal Subsurface Thaw Dynamics of an Aufeis Feature Inferred From Geophysical Methods, J. Geophys. Res.-Earth, 125, e2019JF005345, https://doi.org/10.1029/2019JF005345, 2020.
- Thrush, S. F., Schneider, D. C., Legendre, P., Whitlatch, R. B., Dayton, P. K., Hewitt, hJ. E., Hines, A. H., Cummings, V. J., Lawrie, S. M., Grant, J. P., Pridmore, R. D., Turner, S. J., and McArdle, B. H.: J. Exp. Mar. Biol. Ecol., https://doi.org/10.1016/S0022-0981(97)00099-3, 1997.
- Toohey, R. C., Herman-Mercer, N. M., Schuster, P. F., Mutter, E. A., and Koch, J. C.: Multidecadal increases in the Yukon River Basin of chemical fluxes as indicators of changing flowpaths, groundwater, and permafrost, Geophys. Res. Lett., 43, 12120–12130, https://doi.org/10.1002/2016GL070817, 2016.
- Turetsky, M. R., Abbott, B. W., Jones, M. C., Anthony, K. W., Olefeldt, D., Schuur, E. A. G., Grosse, G., Kuhry, P., Hugelius, G., Koven, C., Lawrence, D. M., Gibson, C., Sannel, A. B. K., and McGuire, A. D.: Carbon release through abrupt permafrost thaw, Nat. Geosci., 13, 138–143, https://doi.org/10.1038/s41561-019-0526-0, 2020.
- Vonk, J. E., Tank, S. E., Bowden, W. B., Laurion, I., Vincent, W. F., Alekseychik, P., Amyot, M., Billet, M. F., Canário, J., Cory, R. M., Deshpande, B. N., Helbig, M., Jammet, M., Karlsson, J., Larouche, J., MacMillan, G., Rautio, M., Walter Anthony, K. M., and Wickland, K. P.: Reviews and syntheses: Effects of permafrost thaw on Arctic aquatic ecosystems, Biogeosciences, 12, 7129–7167, https://doi.org/10.5194/bg-12-7129-2015, 2015.
- Vonk, J. E., Tank, S. E., and Walvoord, M. A.: Integrating hydrology and biogeochemistry across frozen landscapes, Nat. Commun., 10, 1–4, https://doi.org/10.1038/s41467-019-13361-5, 2019.
- Ward, A. S., Zarnetske, J. P., Baranov, V., Blaen, P. J., Brekenfeld, N., Chu, R., Derelle, R., Drummond, J., Fleckenstein, J. H., Garayburu-Caruso, V., Graham, E., Hannah, D., Harman, C. J., Herzog, S., Hixson, J., Knapp, J. L. A., Krause, S., Kurz, M. J., Lewandowski, J., Li, A., Martí, E., Miller, M., Milner, A. M., Neil, K., Orsini, L., Packman, A. I., Plont, S., Renteria, L., Roche, K., Royer, T., Schmadel, N. M., Segura, C., Stegen, J., Toyoda, J., Wells, J., Wisnoski, N. I., and Wondzell, S. M.: Colocated contemporaneous mapping of morphological, hydrological, chemical, and biological conditions in a 5th-order mountain stream network, Oregon, USA, Earth Syst. Sci. Data, 11, 1567–1581, https://doi.org/10.5194/essd-11-1567-2019, 2019.
- Weishaar, J. L., Aiken, G. R., Bergamaschi, B. A., Fram, M. S., Fujii, R., and Mopper, K.: Evaluation of Specific Ultraviolet Absorbance as an Indicator of the Chemical Composition and Reactivity of Dissolved Organic Carbon, Environ. Sci. Technol., 37, 4702–4708, https://doi.org/10.1021/es030360x, 2003.
- Wiens, J. A.: Spatial Scaling in Ecology, Funct. Ecol., 3, 385–385, https://doi.org/10.2307/2389612, 1989.

- Wolock, D. M., Fan, J., and Lawrence, G. B.: Effects of basin size on low-flow stream chemistry and subsurface contact time in the Neversink River watershed, New York, Hydrol. Process., 11, 1273–1286, https://doi.org/10.1002/(SICI)1099-1085(199707)11:9<1273::AID-HYP557>3.0.CO;2-S, 1997.
- Wrona, F. J., Johansson, M., Culp, J. M., Jenkins, A., Mård, J., Myers-Smith, I. H., Prowse, T. D., Vincent, W. F., and Wookey, P. A.: Transitions in Arctic ecosystems: Ecological implications of a changing hydrological regime, J. Geophys. Res.-Biogeo., 121, 650–674, https://doi.org/10.1002/2015JG003133, 2016.
- Yi, Y., Gibson, J. J., Hélie, J.-F., and Dick, T. A.: Synoptic and timeseries stable isotope surveys of the Mackenzie River from Great Slave Lake to the Arctic Ocean, 2003 to 2006, J. Hydrol., 383, 223–232, https://doi.org/10.1016/j.jhydrol.2009.12.038, 2010.
- Yoshikawa, K., Hinzman, L. D., and Kane, D. L.: Spring and aufeis (icing) hydrology in Brooks Range, Alaska, J. Geophys. Res.-Biogeo., 112, G04S43, https://doi.org/10.1029/2006JG000294, 2007.
- Zarnetske, J. P., Bouda, M., Abbott, B. W., Saiers, J., and Raymond, P. A.: Generality of Hydrologic Transport Limitation of Watershed Organic Carbon Flux Across Ecoregions of the United States, Geophys. Res. Lett., 45, 11702–11711, https://doi.org/10.1029/2018GL080005, 2018.

- Zarnetske, J. P., Bowden, W. B., Abbott, B. W., and Shogren, A. J.: High-frequency dissolved organic carbon and nitrate from the Kuparuk River outlet near Toolik Field Station, Alaska, summer 2017–2019, Environmental Data Initiative (EDI) [data set], https://doi.org/10.6073/pasta/990958760c13cdd55b574c5202dc19b7, 2020a.
- Zarnetske, J. P., Bowden, W. B., Abbott, B. W., and Shogren, A. J.: High-frequency dissolved organic carbon and nitrate from the Oksrukuyik Creek outlet near Toolik Field Station, Alaska, summer 2017–2019, Environmental Data Initiative (EDI) [data set], https://doi.org/10.6073/pasta/5d63c098887205597ce0df929467168c, 2020b.
- Zarnetske, J. P., Bowden, W. B., Abbott, B. W., and Shogren, A. J.: High-frequency dissolved organic carbon and nitrate from the Trevor Creek outlet near Toolik Field Station, Alaska, summer 2017–2019, Environmental Data Initiative (EDI) [data set], https://doi.org/10.6073/pasta/3bd6a1d2d9487546f32d46d2943c6e43, 2020c.
- Zimmer, M. A., Bailey, S. W., McGuire, K. J., and Bullen, T. D.: Fine scale variations of surface water chemistry in an ephemeral to perennial drainage network, Hydrol. Process., 27, 3438–3451, https://doi.org/10.1002/hyp.9449, 2013.